

KINEMATICS AND STELLAR POPULATION IN ISOLATED LENTICULAR GALAXIES¹

IVAN YU. KATKOV

Sternberg Astronomical Institute, M.V. Lomonosov Moscow State University, Universitetsky pr., 13, Moscow, 119991 Russia

ALEXEI YU. KNIAZEV

South African Astronomical Observatory, PO Box 9, 7935 Observatory, Cape Town, South Africa
Southern African Large Telescope Foundation, PO Box 9, 7935 Observatory, Cape Town, South Africa and
Sternberg Astronomical Institute, M.V. Lomonosov Moscow State University, Universitetsky pr., 13, Moscow, 119991 Russia

OLGA K. SIL'CHENKO

Sternberg Astronomical Institute, M.V. Lomonosov Moscow State University, Universitetsky pr., 13, Moscow, 119991 Russia and
Isaac Newton Institute, Chile, Moscow Branch
Draft version May 28, 2022

ABSTRACT

By combining new long-slit spectral data obtained with the Southern African Large Telescope (SALT) for 9 galaxies with previously published our observations for additional 12 galaxies we study the stellar and gaseous kinematics as well as radially resolved stellar population properties and ionized-gas metallicity and excitation for a sample of isolated lenticular galaxies. We have found that there is no particular time frame of formation for the isolated lenticular galaxies: the mean stellar ages of the bulges and disks are distributed between 1 and > 13 Gyr, and the bulge and the disk in every galaxy formed synchronously demonstrating similar stellar ages and magnesium-to-iron ratios. Extended ionized-gas disks are found in the majority of the isolated lenticular galaxies, in $72\% \pm 11\%$. The half of all extended gaseous disks demonstrate visible counterrotation with respect to their stellar counterparts. We argue that just such fraction of projected counterrotation is expected if all the gas in isolated lenticular galaxies is accreted from outside, under the assumption of isotropically distributed external sources. A very narrow range of the gas oxygen abundances found by us for the outer ionized-gas disks excited by young stars, $[O/H]$ from 0.0 to +0.2 dex, gives evidence for the satellite merging as the most probable source of this accretion. At last we formulate a hypothesis that morphological type of a field disk galaxy is completely determined by the outer cold-gas accretion regime.

Keywords: galaxies: elliptical and lenticular - galaxies: evolution - galaxies: formation - galaxies: kinematics and dynamics - galaxies: structure.

1. INTRODUCTION

Understanding processes of galaxy formation and evolution is the greatest challenge for modern extragalactic astrophysics. A huge variety of physical processes are involved into galaxy shaping, and it is a key problem to select the dominant agents driving evolution of galaxies of different morphological types.

Lenticular galaxies were introduced by Edwin Hubble (1936) when proposing his famous morphological scheme, ‘Hubble’s fork’, as a hypothetical intermediate type between ellipticals (to the left) and spirals (to the right): the so called S0s placed by him in the centre of the ‘Hubble’s fork’ were to possess large-scale stellar disks as spiral galaxies, but lacked patchy patterns of HII-regions and spiral arms unlike them. Their smooth red-dish appearance implied their resemblance to elliptical galaxies as concerning the stellar populations ages. It was also long been suggested that the intermediate position of the S0s between pure spheroids (elliptical galax-

ies) and disk-dominated late-type spiral galaxies obliged them to have very large bulges. However direct photometric decompositions of the digital images of a representative sample of lenticular galaxies has proved that the bulges of any size can be met in S0s, from very large to tiny ones (Laurikainen, Salo, Buta et al. 2010). So the early idea of Sidney van den Bergh (1976) that within the Hubble’s morphological scheme the S0 galaxies constitute in fact a morphological sequence parallel to the sequence of spiral galaxies, matching their bulge-to-disk ratios at every morphological subtype, becomes now more and more acceptable (Kormendy & Bender 2012; Cappellari, Emsellem, Krajnović et al. 2011). At first glance, this re-forming of the Hubble morphological sequence strengthens the general opinion that S0s may be formed by quenching star formation in the disks of spiral galaxies – this transformation step must be easier to do when the bulge-to-disk ratios are the same in the progenitor and the descendant. But at this point we would like to note that if the bulges of S0s and spirals are indeed similar, the possibility of obtaining a *spiral* galaxy from a *S0 progenitor* arises while this direction of evolution was excluded when the bulges of S0s were supposed to be systematically larger than the bulges of spirals.

A great variety of physical processes that can in prin-

katkov@sai.msu.ru
akniazev@sao.ac.za
olga@sai.msu.ru

¹Based on observations made with the Southern African Large Telescope (SALT), programs 2011-3-RSA.OTH-001, 2012-1-RSA.OTH-002 and 2012-2-RSA.OTH-002.

ciple quench star formation in a disk of a spiral galaxy, to transform it into a lenticular one, are currently discussed: a very incomplete list includes direct collisions (Spitzer & Baade 1951; Icke 1985), tides from a cluster/group dark halo potential (Byrd & Valtonen 1990), ‘harrasment’ – high-speed encounters between galaxies in dense environments (Moore, Katz, Lake et al. 1996), ram pressure by the hot intergalactic medium (Gunn & Gott 1972; Quilis, Moore, & Bower 2000), starvation of star formation because of removing external gas reservoir (Larson, Tinsley, & Caldwell 1980; Shaya & Tully 1984). All these processes are inevitably related to dense environments: it is suggested that only clusters and rich groups of galaxies, having massive dark haloes enclosing many individual galaxies, can provide necessary density of intergalactic medium for effective ram pressure and galaxy tight packing for effective gravitational tides. On one hand, indeed, S0 galaxies are known to be the dominant galaxy population of nearby clusters, their fraction in clusters reaching 60% (Dressler 1980). On the other hand, there is an even larger number of S0 galaxies in the field: the galaxy content of the nearby Universe includes 15% of lenticulars (Naim, Lahav, Buta et al. 1995). Some quite isolated lenticular galaxies even exist (Sulentic, Verdes-Montenegro, Bergond et al. 2006). What are the mechanisms of their formation? Can be they quite different from those acting in dense environments? This question has not even been considered.

Despite the obvious scarcity of possible galaxy transformation mechanisms beyond the clusters and rich groups, it would be erroneous to think that an isolated galaxy evolves as a ‘closed box’. Recently we have studied an isolated early-type spiral galaxy NGC 7217. By analysing a full complexity of its properties including disk structure, dynamical state, inner gas polar disk, and stellar population characteristics along the radius, we have shown that its present structure requires at least two satellite infalls (minor merging) for the last 5 Gyr (Sil’chenko, Chilingarian, Sotnikova et al. 2011). A noticeable gas presence in S0s is not rare, and in particular, off-cluster environments have appeared to favor an external (accretion) origin of this gas (Davis, Alatalo, Sarzi et al. 2011). Moreover, we have shown that in extremely sparse environments, namely, in the quite isolated S0s the warm extended gas is *always* accreted from outside (Katkov, Sil’chenko, & Afanasiev 2014a). So external gas acquisition, related to smooth cold-gas accretion and/or to merging small late-type gas-rich satellites, together with the inner cold-disk instabilities, remain the only possible drivers of isolated lenticular galaxy formation and evolution. By taking this idea in mind, we have undertaken a study of the kinematical and stellar population properties of *isolated* lenticular galaxies, by hoping to single out the evolutionary paths related just to the gas/satellite accretion regime. Here we must also note that the gas accretion and/or minor merging allowed for the field disk galaxies are able not only to quench star formation in a large-scale disk, but to feed and provoke it in the disks where it has not proceeded before (e.g. Birnboim, Dekel, & Neistein (2007); Sancisi, Fraternali, Oosterloo et al. (2008)).

To achieve this goal, we have compiled a list of strictly isolated nearby ($v_r < 4000 \text{ km s}^{-1}$) lenticular galaxies and have undertaken deep long-slit spectroscopy of a

small representative sample of them to study the kinematics of the stars and of the gas and the ages and chemical compositions of the stellar populations as well as the ionization mechanisms and metallicity of the warm-gas component. With these results in hands, we hope to restore formation and evolutionary histories of the isolated lenticular galaxies. In this paper we show and analyze the data on the southern part of the sample: the galaxies having been observed at the Southern Africa Large Telescope (SALT) are presented. The paper is organized as follows: Section 2 describes the sample, Section 3 gives the description of the observations and data reduction, in Section 4 we present our results and discuss them in Section 5, the conclusions drawn from this study are summarized in Section 6.

2. SAMPLE SELECTION

Our approach to compile a sample of strictly isolated lenticular galaxies is based on a set of methods developed in the Laboratory of Extragalactic Astrophysics and Cosmology of the Special Astrophysical Observatory of the Russian Academy of Sciences by Igor Karachentsev, Dmitry Makarov, and their coauthors. They proposed a new group-finding algorithm which was intended to be applied to their Nearby Galaxy Catalog (Karachentsev, Karachentseva, Huchtmeier et al. 2004; Karachentsev, Makarov, & Kaisina 2013). By extending their study of the local large-scale structures, they have also used their algorithms to identify galaxy pairs (Karachentsev & Makarov 2008), triplets (Makarov & Karachentsev 2009), groups (Makarov & Karachentsev 2011), and isolated galaxies (Karachentsev, Makarov, Karachentseva et al. 2011) up to Hubble velocities of $v_r \leq 4000 \text{ km s}^{-1}$. The updated HyperLEDA and NED databases extended by measurements coming from the surveys SDSS, 6dF, HIPASS, and ALFALFA, provided line-of-sight systemic velocities, apparent magnitudes, and morphological types of the galaxies under consideration. The profit of their group-finding approach is that the individual properties of galaxies, in particular an integrated luminosity in the K -band as a stellar mass proxy, are taken into account. They assumed that velocity difference and visible separation of galaxies belonging to a physical pair must both satisfy the condition of negative total energy, and the pair components must be enclosed within the sphere of ‘zero-velocity’ that means that the pair components are separated from the Hubble expansion flow. This algorithm for galaxy grouping is iterative: galaxy-galaxy physical pairs are identified during the first iteration, and after that at the subsequent iterations the galaxy pairs are tied into groups through the common members. The isolation index (II) characterizing isolation degree of any galaxy within the sphere of $v_r \leq 4000 \text{ km s}^{-1}$ is a by-product of all the galaxy grouping procedures. The II value of an unbound galaxy pair is larger than one and indicates a factor by which the mass of one of the components should be increased in order to create a gravitationally bound pair. Correspondingly, the II values of the galaxies belonging to multiple systems are less than one.

Dmitry Makarov has kindly provided us with the information about the isolation indices for all galaxies of the Local Supercluster and its surroundings. To define our sample of isolated lenticular galaxies, we have se-

lected early morphological types, $-3 \leq T \leq 0$, with the isolation indices $II > 2.5$. Also we have taken some galaxies having faint companions with $1 < II < 2.5$ but with the K -magnitude difference of 3 mag and larger having in mind that the low-mass satellites, with the mass of ten percent and less relative to their host, cannot gravitationally affect the evolution of their hosts (unless they merge). The whole sample of the isolated lenticular galaxies, both of the northern and southern skies, lists 281 objects. We have started spectral observations of a representative part of this sample. Firstly, we have carried out spectroscopic observations of 12 northern targets from the sample of isolated S0 galaxies at the 6-m Russian telescope by using universal SCORPIO spectrograph; the results are published in Katkov, Sil'chenko, & Afanasiev (2014a,b). In this paper we present results of the long-slit spectroscopic study of 9 targets of the southern hemisphere undertaken at the Southern African Large Telescope (SALT). As a Discussion, some summary of the results for the unified sample of northern and southern isolated S0s is also given at the end of the paper.

3. LONG-SLIT SPECTROSCOPY

3.1. Observations and data reduction

The observations were performed with the Robert Stobie Spectrograph (RSS; Burgh, Nordsieck, Kobulnicky et al. 2003; Kobulnicky, Nordsieck, Burgh et al. 2003) at the Southern African Large Telescope (SALT) (Buckley, Swart, & Meiring 2006; O'Donoghue, Buckley, Balona et al. 2006). The long-slit spectroscopy mode of the RSS was used with a 1.25 arcsec slit width for the most observations. The total time of one observational block with the SALT is limited by the track-time of about an hour for our targets. For this reason and because the SALT is a queue-scheduled telescope, most of our galaxies were observed more than once and all observations were done during different nights. All observational details are summarised in Table 1. The slit was oriented along the major axis for every galaxy except NGC 7693. The grating GR900 was used for our program to cover finally the spectral range of 3760–6860 Å with a final reciprocal dispersion of $\approx 0.97 \text{ \AA pixel}^{-1}$ and FWHM spectral resolution of 5.5 Å. The seeing during observations was in the range 1.5–3.0 arcsec. The RSS pixel scale is $0''.1267$, and the effective field of view is $8'$ in diameter. We utilised a binning factor of 2 or 4 to give final spatial sampling of $0''.258 \text{ pixel}^{-1}$ and $0''.507 \text{ pixel}^{-1}$ respectively. Spectrum of an Ar comparison arc was obtained to calibrate the wavelength scale after each observation as well as spectral flats were observed regularly to correct for the pixel-to-pixel variations. Spectrophotometric standard stars were observed during twilights, after observations of objects, for the relative flux calibration.

Primary data reduction was done with the SALT science pipeline (Crawford, Still, Schellart et al. 2010). After that, the bias and gain corrected and mosaicked long-slit data were reduced in the way described in Kniazev, Zijlstra, Grebel et al. (2008). The accuracy of the spectral linearisation was checked using the sky line [O I] $\lambda 5577$; the RMS scatter of its wavelength measured along the slit is 0.04 Å. The slit length is approximately

$8'$, so sky spectra from the slit edges were used to estimate the background during the galaxy exposures.

3.2. The Lick index system at the SALT/RSS

To derive stellar population properties from the integrated absorption-line spectra of a stellar system, in particular of a galaxy or its part, one can use the equivalent widths (EWs) of the stellar absorption spectral lines. Lick indices (Faber, Friel, Burstein et al. 1985; Worthey, Faber, Gonzalez et al. 1994; Worthey & Ottaviani 1997) is a uniform, strictly established system of set line parameters measured in part as EWs of strong absorption lines in the spectral range of 4000–6200 Å. The system is named after a 20-yr spectral survey of nearby galaxies and stars with the 3-m Lick telescope using a photon-counting detector IDS at the Cassegrain spectrograph. The line and continuum border definitions within the Lick system are tied to the spectral resolution of the Lick spectrograph, $\approx 8 \text{ \AA}$ but slightly varying with wavelength. The aim was to include the spectral lines fully into the integrated spectral ranges. The necessity to apply the Lick definitions of the absorption-line EW measurements to galactic spectra was strengthened by the fact that many evolutionary synthesis models of simple stellar populations, starting from the work of Worthey, Faber, Gonzalez et al. (1994), used calibrations of the *stellar* Lick indices on the stellar effective temperatures and metallicities as their input data. These calibration relations were obtained from observations of more than 460 nearby stars with exactly the same Lick spectral setup.

The Volume Phase Holographic (VPH) grating of 900 g/mm of the SALT/RSS has a spectral resolution of about 5.5 Å that differs from the standard Lick resolution, $\approx 8 \text{ \AA}$. We hence need to calibrate the instrumental absorption-line indices obtained from the RSS spectra by integrating the spectral fluxes in the bands prescribed by the Lick system to the standard Lick system. This was done by observing a sample of Lick standard stars visible in southern sky from the list of Worthey, Faber, Gonzalez et al. (1994). In total, 10 giant and dwarf stars with spectral types in-between F4 and K4 were observed with the VPH900 grating and the slit width of 1.25 arcsec. All observations of these bright stars were done either within twilight time or during bright moon time with poor seeing and cloudy conditions. For all obtained spectra we calculated the instrumental-system Lick indices $H\beta$, Mgb, Fe5270, and Fe5335, by integrating fluxes within the prescribed wavelength intervals for the lines, as well as their blue and red continuum points, as recommended by Worthey, Faber, Gonzalez et al. (1994).

The instrumental-system Lick indices were then compared to the tabular values provided by Worthey, Faber, Gonzalez et al. (1994). The linear dependencies between the two sets of data were recovered, and the linear regressions were calculated, and are also shown in Fig. 1:

$$H\beta(\text{Lick}) = (1.084 \pm 0.060) \times H\beta(\text{RSS}) - (0.146 \pm 0.158),$$

the rms scatter of the points around the straight line is 0.20 Å.

$$\text{Mgb}(\text{Lick}) = (1.091 \pm 0.069) \times \text{Mgb}(\text{RSS}) - (0.077 \pm 0.189),$$

Table 1
Long-slit spectroscopy of studied galaxies.

Galaxy	Date	Exp. [sec]	Binning	Slit [arcsec]	PA(slit) [deg]	Seeing [FWHM, arcsec]
IC 1608	07.11.2012	620x3	2x4	1.25	350	2.0
	04.01.2013	620x3	2x4	1.25	350	2.0
IC 4653	11.05.2012	1200x3	2x2	1.25	52	2.0
NGC 1211	05.10.2011	820x3	2x2	1.25	210	3.0
	22.11.2011	900x3	2x2	1.25	210	3.0
	22.12.2011	1030x2,730	2x2	1.25	210	3.0
	25.12.2011	1000x3	2x2	1.25	210	3.0
NGC 2917	17.12.2012	900x2	2x4	1.25	169	3.0
	06.01.2013	900x3	2x4	1.25	169	3.0
	15.01.2013	900x3	2x4	1.25	169	3.0
	15.02.2013	900x2,700	2x4	1.25	169	3.0
NGC 3375	17.02.2012	850x2,472	2x2	1.25	130	2.0
	23.02.2012	800x3	2x2	1.25	130	2.0
	28.02.2012	800x3	2x2	1.25	130	2.0
NGC 4240	14.01.2013	600x3	2x4	1.25	283	2.0
	19.03.2013	600x3	2x4	1.25	283	2.0
NGC 6010	05.04.2013	750x3	2x4	1.00	105	2.0
NGC 7693	10.07.2012	650x3	2x2	1.25	210	2.0
	04.09.2012	650x3	2x2	1.25	30	2.0
	22.09.2012	650x3	2x2	1.25	30	2.0
UGC 9980	10.06.2012	700x3	2x2	1.25	175	2.0
	10.07.2012	650	2x2	1.25	175	2.0

the rms scatter of the points around the straight line is 0.34 Å.

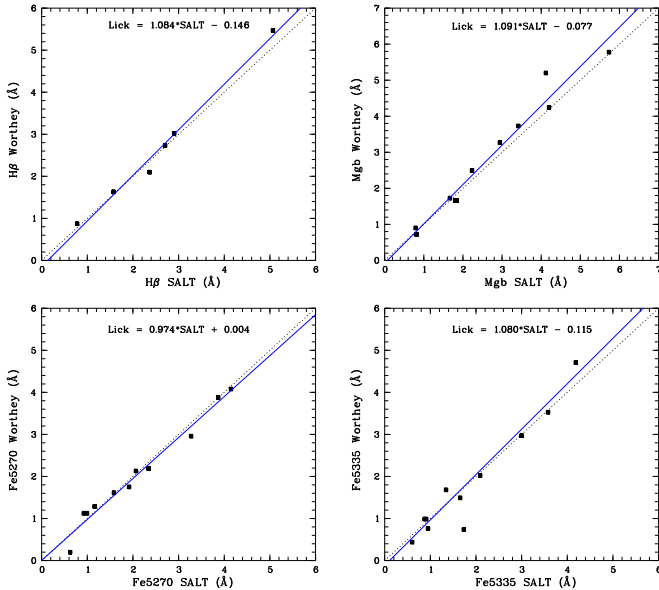


Figure 1. The calibration of the instrumental Lick indices of the RSS/SALT with grating VPH900 onto the standard Lick system. The straight solid lines are the best-fit relations while the dashed lines are the equality relations.

$$\text{Fe5270(Lick)} = (0.974 \pm 0.053) \times \text{Fe5270(RSS)} + (0.004 \pm 0.113),$$

the rms scatter of the points around the straight line is 0.20 Å.

$$\text{Fe5335(Lick)} = (1.080 \pm 0.059) \times \text{Fe5335(RSS)} - (0.115 \pm 0.116),$$

without HD 10700, with the remaining 9 stars, the rms scatter of the points around the straight line is 0.22 Å.

Comparing the derived rms scatter of the individual stars around the best-fit straight lines with the mean accuracy of the tabular Lick indices mentioned by Worthey, Faber, Gonzalez et al. (1994), namely 0.22 Å for H β , 0.23 Å for Mgb, 0.28 Å for Fe5270, and 0.26 Å for Fe5335, we conclude that the scatter of the points in the plots of Fig. 1 is produced mostly by the errors of the tabular indices.

3.3. Full spectral fitting

Besides the Lick index measurements, we have also applied full spectral fitting approach to our spectra; it is valuable when strong emission lines are present in spectra, and the age-sensitive index H β is strongly contaminated by the Balmer emission.

In order to perform full spectral fitting of the synthetic spectra to the observed data, we have used an IDL-based package NBURSTS (Chilingarian, Prugniel, Sil'Chenko et al. 2007a,b). This package implements a pixel-space fitting algorithm, that involves the non-linear least-squares optimization using Levenberg-Marquardt algorithm. The observed spectrum is approximated by a stellar population model broadened by line-of-sight velocity distribution (LOSVD); the parameters of the stellar population model, metallicity and age, are determined during the same minimization loop as the internal

kinematical parameters – line-of-sight velocity and stellar velocity dispersion.

In our study, we use intermediate spectral resolution ($R=10000$) simple stellar population (SSP) models generated by evolutionary synthesis code PEGASE.HR (Le Borgne, Rocca-Volmerange, Prugniel et al. 2004) in a wavelength range 3900-6800 Å for the Salpeter (1955) initial mass function based on ELODIE3.1 stellar library (Prugniel, Soubiran, Koleva et al. 2007). The grid of synthetic SSP spectra was pre-convolved with spectral line spread function (LSF) of the RSS spectrograph, which was determined by fitting spectrum of one of Lick standard stars against the $R=10000$ spectrum for the same star taking from ELODIE3.1 library. During the main minimization loop the template spectrum is extracted from the grid of models by interpolation to the current age T and metallicity $[Z/H]$. Then template is convolved with LOSVD, which is defined by Gauss-Hermite series of orthogonal functions with parameters v , σ , h_3 , h_4 (van der Marel & Franx 1993). The model includes a multiplicative continuum aimed to take into account flux calibration uncertainties both in observations and in the models as well as possible dust attenuation of galactic spectrum.

In order to avoid systematic errors in the solution we masked narrow 15 Å– wide regions around ionized-gas emission lines and around traces of the subtracted strong airglow lines. As shown by Chilingarian, Prugniel, Sil’chenko et al. (2007a) and Chilingarian (2009), excluding age-sensitive Balmer lines from the full spectral fit neither biases age estimates nor significantly degrades the quality of the age determination. To achieve the required signal-to-noise ratio of 20-30 per spatial bin, we performed adaptive binning of the long-slit spectra along the slit.

A number of similar approaches of the full spectral fitting techniques exist, for instance PPF by Cappellari & Emsellem (2004), STARLIGHT by Cid Fernandes, Mateus, Sodré et al. (2005), STECKMAP by Ocvirk, Pichon, Lançon et al. (2006), and other packages. The main difference between the NBURSTS package and the current version of the popular PPF code as well as STARLIGHT and STECKMAP is that the NBURSTS specifies template spectrum as a single SSP spectrum with age and metallicity as free parameters. Other packages construct template spectrum as a linear combination of SSPs with fixed ages and metallicities and SSP weights taken as free parameters. In these cases the star formation history can be in principle derived from the observed galaxy spectra, but that requires very high signal-to-noise spectra (Ocvirk, Pichon, Lançon et al. 2006). Indeed, insufficient signal-to-noise level of spectra leads to degeneracy between weights of the different SSPs and unreliable star formation history. Due to understanding this effect, the majority of studies where linear combination of SSPs are used provide only mass- and/or light-weighted SSP-equivalent parameters of stellar populations that correspond to NBURSTS fitting parameters by definition.

3.4. Final choice of the stellar population parameters

To derive the stellar population parameters, we have tried both approaches: we have fitted ‘pixel-by-pixel’ all our spectra along the slit and we have calculated the

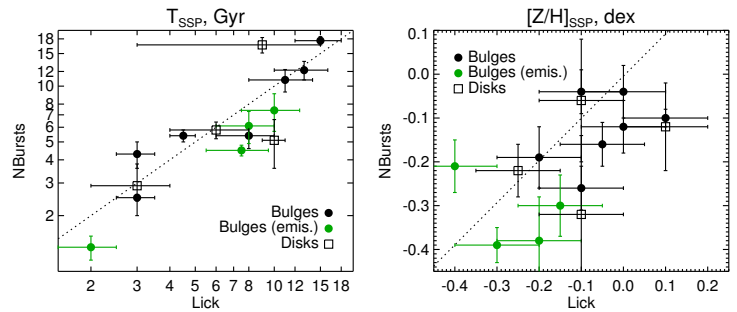


Figure 2. The comparison of the ages and metallicities derived by two different methods: by full spectral fitting using the PEGASE stellar population models (‘NBursts’) and through the Lick indices $H\beta$ and $[MgFe]$ using the models by Thomas, Maraston, & Bender (2003). The dotted line represents the equality locus. Filled circles correspond to measurements in the bulges, open squares - to disks. Green circles show bulges with presence of emissions in the spectra.

Lick indices $H\beta$, Mgb, Fe5270, and Fe5335. The full spectral fitting included the use of the evolutionary synthesis code PEGASE.HR (Le Borgne, Rocca-Volmerange, Prugniel et al. 2004). The measured Lick indices were confronted to the models by Thomas, Maraston, & Bender (2003) allowing to analyze magnesium-overabundant stellar populations. To obtain the stellar magnesium-to-iron ratios, we were restricted to the use of Lick indices only, because the full spectral fitting assumed solar abundance ratios. On the other hand, the full spectral fitting has great advantage in deriving the stellar population ages when we deal with the spectra containing strong Balmer emission lines: when the Lick index $H\beta$ is contaminated by the hydrogen emission line, the full spectral fitting is much more safe because it allows to exclude spectral ranges polluted by emission lines. By calculating the Lick index $H\beta$, we tried to correct it for the emission by applying our approach basing on the measurements of the $H\alpha$ emission-line equivalent width (Sil’chenko 2006); however when the emission is strong, and the ionized-gas excitation is uncertain, the correction cannot be perfect. Unfortunately, among our southern sample of the isolated S0s, almost all galaxies demonstrate rich emission-line spectra. So for the present sample in particular we shall analyze mostly the results on the ages and metallicities obtained through the full spectral fitting. However, we wonder to know if two approaches give consistent results, and for a few our galaxies with weak or absent emission lines we have compared the ages and metallicities of the bulges and disks obtained by full spectral fitting using the PEGASE stellar population models with those obtained through the Lick indices $H\beta$ and $[MgFe]$ using the models by Thomas, Maraston, & Bender (2003). To get a sufficient statistical level of the comparison, we have involved the results for our previous sample of the northern isolated S0s (Katkov, Sil’chenko, & Afanasiev 2014b), and the final comparison can be inspected in Fig. 2. The ages are consistent within the accuracy of their determination, and the metallicities may have a systematic shift by some 0.1 dex, perhaps due to slightly non-solar magnesium-to-iron ratios of the stellar populations in the S0s studied by us.

3.5. Ionized gas

A warm-gas emission-line spectrum can be obtained by subtracting the stellar component contribution (i.e., the best-fitting stellar population model) from the observed spectrum at every spatial bin. The resulted pure emission-line spectra are uncontaminated by absorption lines of the stellar components that is especially important for the Balmer lines. Then we fitted emission lines with Gaussians pre-convolved with the instrumental LSF in order to determine the LOS velocities of the ionized gas and emission-line fluxes.

4. RESULTS

By applying the above-mentioned techniques to every galaxy spectrum along the major axis, we have derived the radial profiles of the following characteristics: stellar rotation velocity, stellar velocity dispersion, SSP-equivalent stellar ages, metallicities, and magnesium-to-iron ratios, ionized-gas rotation velocity, warm-gas velocity dispersion, emission-line flux ratios. The latter characteristics can be plotted at the classical excitation-diagnostic diagrams, so called BPT (after Baldwin, Phillips, & Terlevich) (Baldwin, Phillips, & Terlevich 1981), to identify the gas excitation mechanism. If we see that the gas is ionized by young stars, we can apply so called ‘strong-line calibrations’ to estimate the gas metallicity. We have explored the formulae from the paper by Pettini & Pagel (2004) and have estimated oxygen abundance using emission-line indices $O3N2 = \log_{10}(((O III)\lambda 5007/H\beta)/([N II]\lambda 6583/H\alpha))$ and $N2 = \log_{10}([N II]\lambda 6583/H\alpha)$ which are calibrated by Pettini & Pagel (2004) against $12 + \log(O/H)$ by using the data on 137 HII-regions with known electronic temperatures. In the case of very noisy H β and [OIII] emission lines we used another calibration from Pettini & Pagel (2004) that involves only N2 index. Due to exploration of ratios of nearest emission lines the dust attenuation does not affect the oxygen abundance estimations.

Below we present the results for every galaxy in graphical way and give brief description of the individual properties of the galaxies.

IC 1608. It is one of the most luminous galaxies of our sample. The galaxy demonstrates fast stellar rotation; however the stellar disk is rather hot dynamically, $\sigma_* \geq 100 \text{ km s}^{-1}$. The galaxy is very gas-rich; we observe strong emission lines over the full slit extension. The nuclear emission-line spectrum is a typical LINER-like one; starting from the radius of about 10 arcsec, the ionized gas is excited mostly by young stars, and in the outer part, $R \approx 40''$, a starforming ring is clearly seen. The gas subsystem looks cold only within the starforming ring; elsewhere in the disk the gas velocity dispersion matches that of stars. The gas rotation curve coincides exactly with the stellar one so we can be sure that the gas is confined to the main galaxy plane. The gas oxygen abundance at $R > 30''$ is observed to be nearly solar or slightly higher while the stellar mean metallicity there is very poor, about $-0.6 \div -0.9$ dex. The magnesium-to-iron ratio in the stellar component is homogeneous along the radius and close to $+0.1$ dex; the mean stellar age looks intermediate, 3–5 Gyr, over the whole galaxy too. We may so suspect that low-level starforming events like the current one have occurred multiple times during the galaxy evolution for the last

several billion years; perhaps they have been provoked by small gas-rich satellites merging.

IC 4653. This dwarf galaxy is classified as SB0/a pec in the NED² database. However despite this relatively late morphological type and the elongated isophote shape, our spectrograph slit aligned with the isophote major axis reveals very weak rotation and rather large stellar velocity dispersion. We would re-classified the galaxy as a dwarf elliptical one and exclude it from the further consideration of our sample of isolated lenticular galaxies. Interestingly, the strong emission lines excited by the current star formation are seen over the whole galaxy including its nucleus.

NGC 1211. This luminous, almost face-on galaxy has a bar and two rings – the inner reddish one at $R \approx 20''$ and the blue starforming outer one at $R \approx 60''$. Surveys in the 21 cm line reported earlier large neutral hydrogen content in this galaxy, 5.5 billion solar masses of HI (Garcia-Appadoo, West, Dalcanton et al. 2009), so the strong emission lines were also expected in its optical spectrum. The discrepancy between the rotation velocities of the ionized gas and the stars at $R < 10''$ can be explained both by asymmetric drift and bar influence; beyond the radius of $10''$ the ionized gas and stars rotate together, and we conclude that the gas is confined to the main galaxy plane. The gas is excited by the LINER-like nucleus and by shock waves (from the bar?) in the central part of the galaxy, at $R < 10''$, and by young stars beyond this radius; the oxygen abundance of the gas in the outer starforming ring is the solar one. Mean-time the low-surface brightness stellar disk at $R \approx 30''$ demonstrates very old age, $T \geq 10$ Gyr, and very low stellar metallicity, $[Z/H] \approx -1.5$ dex. The bulge and the lens which we relate to the bar ends, demonstrate intermediate stellar ages and strong metallicity gradient along the radius.

NGC 2917. This very luminous S0⁺ galaxy is strongly inclined to the line of sight, but is not exactly edge-on, so we can distinguish a dust ring and no signs of bar in the galaxy. The bulge is so small that the galaxy has been included into the list of ‘flat’ late-type galaxies by Mitronova, Karachentsev, Karachentseva et al. (2004). The systemic velocity of NGC 2917 given in the NED, 3675 km s^{-1} , is erroneous coming from a very weak spurious 21-cm signal detected by Richter & Huchtmeier (1987). Our optical spectral observations give $v_{sys} = 5377 \text{ km s}^{-1}$ for this galaxy, so the galaxy is even more luminous than it has been thought before. Though we have traced the stellar component of NGC 2917 almost up to its optical border, $R_{25} = 38''$ (RC3³), we have only measured its lens; the outer stellar disk is very low-surface brightness one and could not be detected in our observations. While the bulge has intermediate stellar-population characteristics, the lens looks rather young, $T = 2 - 3$ Gyr, that is consistent with the ionized gas excited by current star formation at $R \geq 10''$. The ionized-gas metallicity is high. The fall of the ionized-gas rotation velocity at the southern edge of the galaxy accompanied by the rise of the velocity dispersion of the gas clouds seems to be real. Are there any traces of in-

² NASA/IPAC Extragalactic Database

³ Third Reference Catalogue of Bright Galaxies.

teraction?

NGC 3375. Another galaxy which being previously classified as a lenticular one is in fact an elliptical: its stellar component does not rotate regularly, and the stellar velocity dispersion exceeds 150 km s^{-1} everywhere through the galaxy. Emission lines are absent in the spectrum.

NGC 4240. The galaxy is classified in RC3 as between E and S0 ($T = -3.8 \pm 0.5$). In the frame of the APM survey (Naim, Lahav, Buta et al. 1995) when 6 independent researchers classified it ‘by eye’, three voted for S0 and three voted for E (see ‘Detailed classification’ option in the NED). However our long-slit cross-section along the major axis reveals rather fast rotation of the stellar component; and in the photometric data we see an exponential disk at $R > 15''$. So we consider NGC 4240 as a lenticular galaxy. The stellar population properties were spectrally studied by Reda, Proctor, Forbes et al. (2007) up to the distance about $10''$ from the center; a slightly subsolar metallicity and a rather old age were measured by the Lick index method. The kinematics was examined by Hau & Forbes (2006); however their slit was obviously off the dynamical center, and they did not report gas counterrotation for this galaxy which is striking. We have traced the stellar rotation and stellar population properties toward $R \approx 25''$ so measuring not only the bulge but also the large-scale stellar disk at $R > 15''$. Both the bulge and the disk have an intermediate stellar age, about 5 Gyr, but the disk is very metal-poor, $[Z/H] \approx -1.0$, while the bulge has only $[Z/H] \approx -0.3$. The ionized gas counterrotates the stars in the bulge-dominated area; while the stellar velocity dispersions of the stars and gas clouds are comparable, the rotation velocities differ significantly, and we conclude that the ionized gas may rotate in the plane which does not coincide with the plane of the stellar disk. The gas metallicity in the outer starforming ring, at $R \approx 15''$, is close to the solar one.

NGC 6010. It is another small-bulge, edge-on S0 galaxy included into the catalogue of ‘flat galaxies’ by Mitronova, Karachentsev, Karachentseva et al. (2004). Also we must note that in our present sample it is the only S0-galaxy without strong emission lines in the spectra. We see only weak narrow emission lines with LINER-like excitation in the very circumnuclear region; some signs of the ionized-gas counterrotation are however detected. Meantime the neutral hydrogen is found in this galaxy by Springob, Haynes, Giovanelli et al. (2005), but no signs of recent star formation are present. The stellar ages of the nucleus ($T = 9$ Gyr) and of the bulge ($T = 8$ Gyr) are slightly older than in other galaxies of our sample. However, the characteristics of the disk in the radius range $R = 20'' - 40''$ are quite typical – $T = 5$ Gyr and $[Z/H] = -0.4$.

NGC 7693. Due to instrumental problems, the galaxy was observed with the slit turned by some 40 degree to the major axis. However, even so, the observed stellar rotation is too slow, and the ionized-gas velocities are quite decoupled from the stellar ones. Consequently, no signs of current star formation is seen in this galaxy, though both the bulge and the disk look very young, 1–3 Gyr old. The magnesium-to-iron ratio over the whole galaxy is solar so it seems that continuous star formation ceased rather recently, due to perhaps just minor merger from

an inclined orbit.

UGC 9980. The galaxy demonstrates fast regular rotation, looking quite similar in the stellar and ionized-gas components. The gas is spread over the whole galaxy, and starting outward from the radius $R > 10''$ it is excited by young stars. However, both the bulge and the large-scale stellar disk possess rather old stellar populations, $T = 7$ Gyr in the former and $T = 10$ Gyr in the latter, so the widespread star formation has evidently started quite recently: unless the case of NGC 7693, this time minor merging has stimulated star formation, not ceased it. The difference of metallicities – $[Z/H] = -1.0$ dex in the stellar disk and -0.2 dex in the gaseous disk – indicates also the external origin of the current fuel for the star formation. The inner stellar ring related to ansae at the ends of the bar, at $R \approx 10''$, is distinguished by slightly younger stellar age, $T \approx 5$ Gyr. However, this ancient ring-like star formation burst was probably related not to interaction but to the bar affecting gaseous disk of the galaxy which was perhaps more gas-rich at $z = 0.5$ than it is at the present epoch.

After obtaining the full radial profiles of the stellar characteristics in the galaxies studied, which are presented in the Appendix, we have wished to extract mean characteristics for the large-scale galaxy components – bulges and disks. To identify radius ranges that correspond to the bulge and disk domination in the integrated light, we have undertaken photometric decomposition of the images of the galaxies. For this purpose we have used mostly the SDSS public database, Data Release 9; the r -band images as the images with the highest signal-to-noise ratio have been taken. For the southern galaxy NGC 4240 which was not observed in the frame of the SDSS we have decomposed the 2MASS composite, $J + H + K$, image. For one galaxy, IC 1608, very deep gri photometric data obtained during test observations of the LCOGT project (Sil’chenko, Kniazev, & Chydakova 2015). For every galaxy, we have performed an isophotal analysis and have derived azimuthally-averaged surface-brightness radial profiles. By inspecting these profiles, we have found the outer radial segments where the surface-brightness radial profiles can be well approximated by exponential laws, and the isophote ellipticity stays constant. These outer parts of galaxies are identified by us as disk-dominated. To characterize the bulges which are mostly compact in the galaxies of our sample we fix the radial range of $4'' - 7''$ that is beyond the unresolved nucleus contamination under our seeing conditions. In some galaxies we have also distinguished the radial ranges where we see rings of enhanced stellar brightness or flat brightness profile segments betraying the presence of lenses. The corresponding segments for each component are shown by shaded gray lines in figures in the Appendix. The mean stellar ages, metallicities, and magnesium-to-iron ratios for the bulges, disks, rings, and lenses of the galaxies studied here are presented in the Table 2.

5. DISCUSSION

In this paper we have described the results of spectral study for 7 isolated lenticular galaxies of the southern sky (another 2 galaxies observed so far have been re-classified here as ellipticals basing on their stellar kinematics and

Table 2
Average stellar population parameters.

Galaxy	N(bins)	T, Gyr	[Z/H], dex	[Mg/Fe], dex	σ , km/s
Bulge					
IC 1608	4	4.7 \pm 0.3	-0.21 \pm 0.07	0.12 \pm 0.09	149 \pm 9
NGC 1211	3	4.5 \pm 0.4	-0.16 \pm 0.05	0.11 \pm 0.07	156 \pm 18
NGC 2917	4	6.1 \pm 1.3	-0.21 \pm 0.06	0.27 \pm 0.08	191 \pm 4
NGC 4240	4	4.6 \pm 0.3	-0.32 \pm 0.08	0.18 \pm 0.09	108 \pm 11
NGC 6010	4	8.16 \pm 0.45	-0.19 \pm 0.07	0.19 \pm 0.06	154 \pm 11
NGC 7693	8	1.35 \pm 0.18	-0.38 \pm 0.10	-0.02 \pm 0.02	82 \pm 14
UGC 9980	6	7.4 \pm 1.4	-0.30 \pm 0.07	0.18 \pm 0.11	138 \pm 20
Disk					
IC 1608	8	3.5 \pm 0.8	-0.46 \pm 0.14	0.18 \pm 0.15	138 \pm 32
NGC 1211	2	10.5 \pm 4.1	-1.50 \pm 0.14	...	141 \pm 12
NGC 2917	0
NGC 4240	5	5.4 \pm 2.1	-1.02 \pm 0.11	0.33 \pm 0.13	112 \pm 8
NGC 6010	12	5.4 \pm 2.4	-0.36 \pm 0.16	0.18 \pm 0.04	113 \pm 21
NGC 7693	11	1.5 \pm 0.9	-0.67 \pm 0.21	0.15 \pm 0.13	106 \pm 24
UGC 9980	5	9.8 \pm 2.8	-0.99 \pm 0.12	0.21 \pm 0.20	83 \pm 5
Lens/Ring/Plateau					
IC 1608	10	4.6 \pm 2.8	-0.77 \pm 0.20	0.24 \pm 0.08	98 \pm 5
NGC 1211	12	5.6 \pm 2.7	-0.82 \pm 0.23	0.20 \pm 0.18	148 \pm 38
NGC 2917	10	2.6 \pm 0.6	-0.34 \pm 0.08	0.24 \pm 0.07	130 \pm 21
NGC 4240	0
NGC 6010	0
NGC 7693	0
UGC 9980	7	4.6 \pm 2.2	-0.48 \pm 0.18	0.22 \pm 0.19	114 \pm 8

do not take part in the analysis below). Earlier we have already published the results of the similar study for 11 isolated lenticulars of the northern sky which were observed at the Russian 6m telescope using the SCORPIO and SCORPIO-2 spectrograph (Katkov, Sil'chenko, & Afanasiev 2014a,b). With the totality of 18 isolated lenticular galaxies observed with the long-slit spectrographs of two large telescopes, we can now discuss some statistical properties concerning the kinematics, the stellar population parameters, and the ionized-gas features in isolated lenticular galaxies. The overall distributions of the parameters of the stellar component for the bulges, disks, and rings/lenses are presented for the total sample in Fig. 3. The distribution of the absolute magnitudes in *B*- and *K*-band are shown in Fig. 4.

5.1. Bulges vs. Disks

Fig. 5 demonstrates first of all the dynamical status of the bulges and disks in our sample of isolated lenticular galaxies. The diagrams presented in the two left plots for the disks and for the bulges correspondingly, confront the ratio of the regular rotation velocity to the stellar velocity dispersion versus the visible ellipticity of the isophotes. It was proposed by Illingworth (1977) and theoretically calculated by Binney (1978b,a) to check if the shape of a galaxy spheroid is supported by rotation. The main theoretical locus at this diagram signifies so called oblate spheroids – ones round in the equatorial plane, with isotropic velocity dispersion, whose smaller third axis is completely explained through flattening by rotation. Many true elliptical galaxies are found well below this locus because they rotate too slowly, and their shapes are supported by anisotropy of the velocity dispersion distributions. Jonh Kormendy (1993) (see also Kormendy & Kennicutt (2004) for the updated version of this diagram) used this diagram for the bulges of disk

galaxies to separate so called ‘classical bulges’ which can be considered as analogues of elliptical galaxies, from the ‘pseudobulges’ which reveal the disk-like kinematics. If the observed characteristics place some bulges above the theoretical line for oblate spheroids, we would classify them as ‘pseudobulges’ formed from the disk material during secular dynamical evolution. Fig. 5, middle plot, gives evidence for the roughly equal proportion of ‘classical bulges’ and ‘pseudobulges’ among the isolated lenticular galaxies: the points are oscillating around the theoretical locus for the oblate isotropic spheroids. When inspecting Fig. 5 (right plot), we make sure again that in 8-10 bulges of 18 the stellar velocity dispersion is the same as in the surrounding disks so indeed these are ‘pseudobulges’.

Fig. 6 gives comparison of the characteristics of the stellar populations in the bulges and in the disk structures: it is the comparison of age–age, metallicity–metallicity, Mg/Fe ratio–Mg/Fe ratio. The first and the third plots demonstrate correlations between the properties of the bulges and of the disks: covering all the range of possible ages, from 1 Gyr to 17 Gyr, the mean stellar ages of the bulges and disks tend to be similar in the galaxies studied, and the magnesium-to-iron ratios are strictly the same in the bulges and in the disk structures. It is an opposition to the properties of S0 galaxies in denser environments: Sil'chenko, Proshina, Shulga et al. (2012) found for a sample of mostly group S0 members that the disks appear to be usually older than the bulges covering homogeneously the upper left corner of the diagram similar to the Fig. 6 (left plot), and Johnston, Aragón-Salamanca, & Merrifield (2014) have found just the same effect for all the Virgo S0s studied by them. In both dense-environment samples the stellar disks appear to be much more magnesium-overabundant than the bulges. We can conclude that when placed

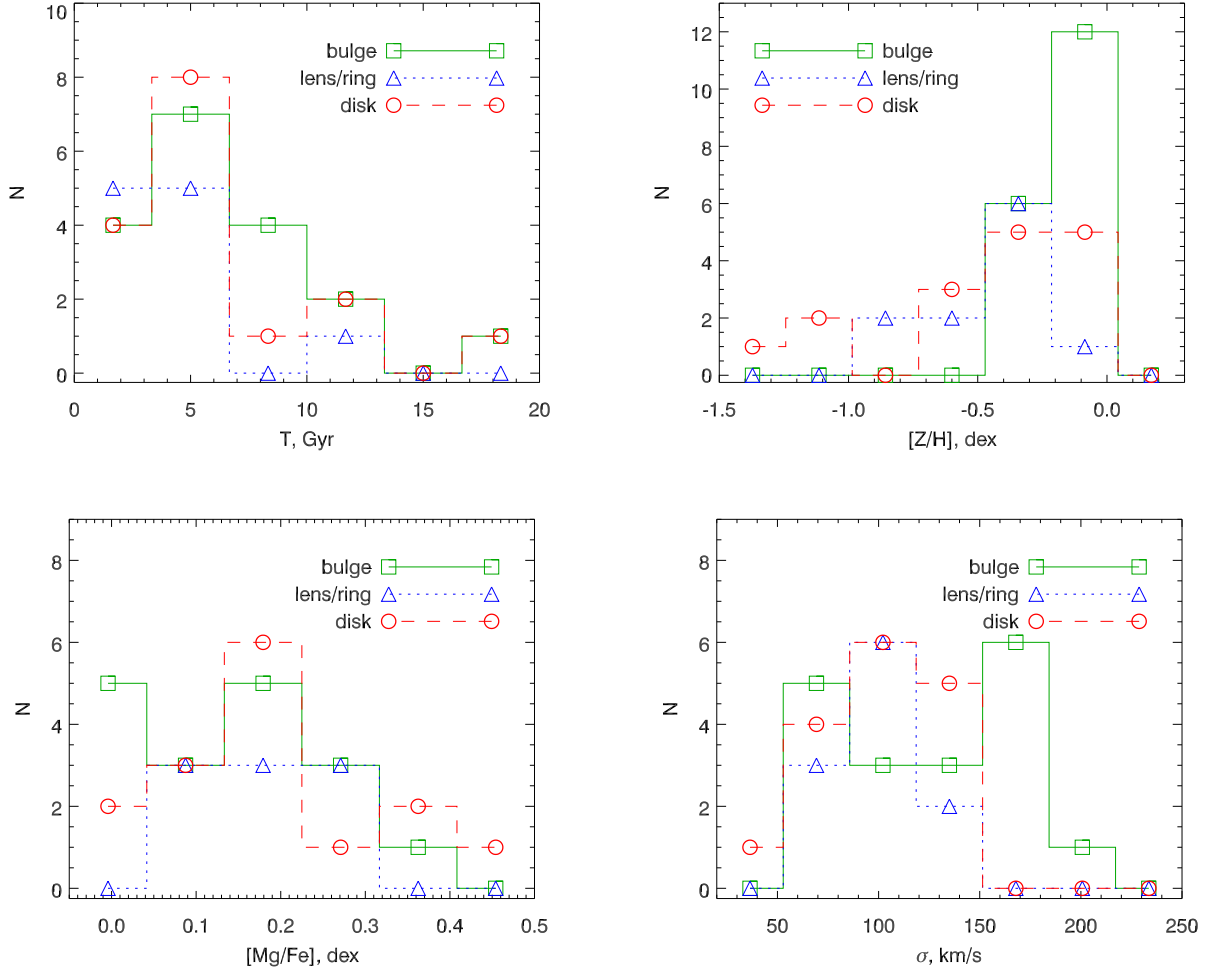


Figure 3. Distributions of our complete sample of the isolated lenticular galaxies over the found parameters of the stellar populations for every structural component – bulges, disks, rings or lenses.

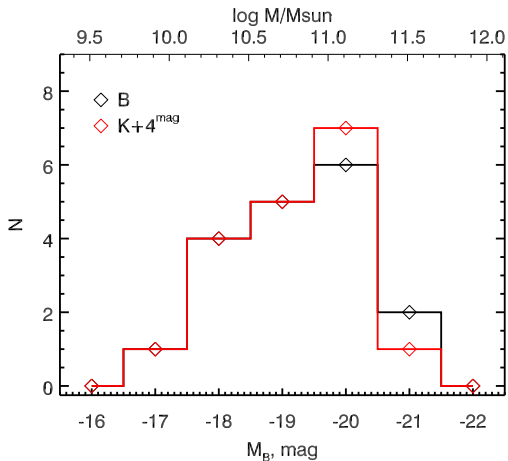


Figure 4. Histogram of integrated absolute magnitudes in B-band (black line) and shifted by 4^m K-band (red line) for the total SALT & SCORPIO sample of the isolated lenticular galaxies. Corresponding stellar masses are shown in the upper x-axis and were calculated by using $M/L_K = 1$.

beyond the outer gravitational and hot-medium influence, the bulges and the disks in S0 galaxies formed syn-

chronously: star formation started simultaneously here and there and ceased at one moment. Interestingly, despite the synchronous star formation, the mean stellar metallicities of the disk structures are significantly lower than the metallicities of the bulges (Fig. 6, middle plot). Does it mean that pristine outer gas was accreted by the outer disks and fueled star formation there, while the nearly simultaneous star formation in the bulges was fed by the gas pre-processed and enriched in the disks?

Let us inspect some scaling relations connecting evolutionary and dynamical characteristics of the stellar components which are commonly studied for the elliptical galaxies. Fig. 7 (left plot) confronts the mean stellar ages of the different structural components with their magnesium-to-iron ratio which characterizes the duration of the main starforming episode, from a very brief, shorter than 10^9 years ($[Mg/Fe] = +0.3$), to several Giga-years ($[Mg/Fe] = 0.0$). We see a cloud of points limited at the down right by a linear law which marks probably the initial epoch of launching star formation in S0s at $z \approx 3$: star formation starting 12 Gyr ago and ceasing just immediately would give $[Mg/Fe] = +0.3$, and star formation starting 12 Gyr ago and lasting to 4 Gyr ago would give $[Mg/Fe] = 0.0$. However there is a lot

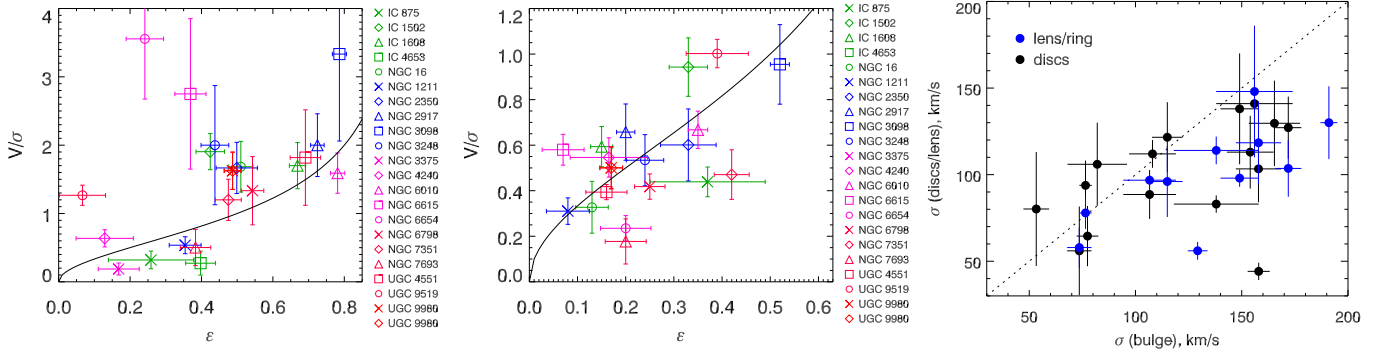


Figure 5. Dynamical diagnostics diagrams: ellipticity vs. V/σ for the disks (*left*), the same for the bulges (*center*), and comparison of the stellar velocity dispersions in the bulges and disks (*right*). The solid line shows the locus of oblate spheroids, which can be considered as demarcation line between disk-like and spheroid-like system.

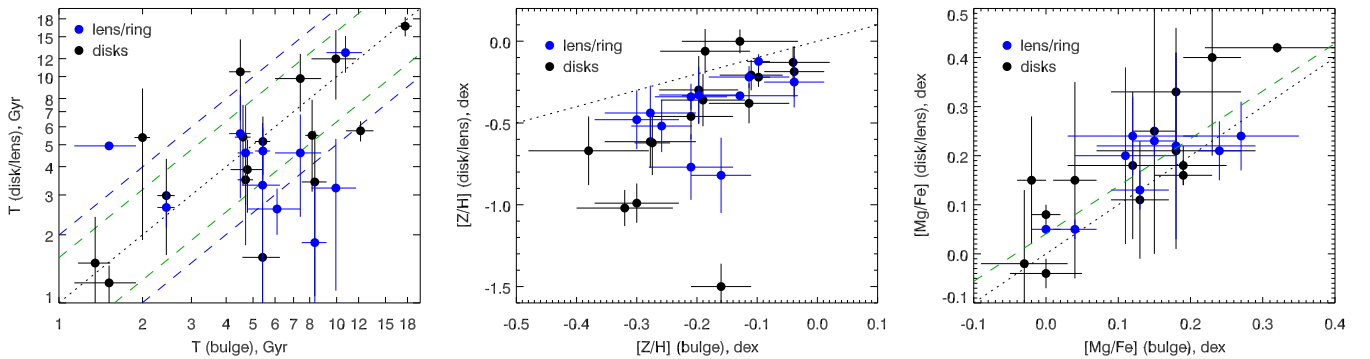


Figure 6. Comparison of the stellar populations in the bulges and in the disks: Age–age diagram (*left*), metallicity–metallicity diagram (*center*), and $[\text{Mg}/\text{Fe}] - [\text{Mg}/\text{Fe}]$ (*right*). Green and blue dashed lines in the left panel correspond to deviation from bisector (dotted line) of value ± 0.2 dex (by 1.5 times) and ± 0.3 dex (by 2 times), respectively. Dotted lines show equality line. Green dashed line in the right panel shows linear fit of measurements.

of points, relating both to the bulges and to the disks, which are expanding to the left of this limiting line. Obviously these are the stellar systems which have started their formation much later than at $z = 2 - 3$: to get the mean stellar age of 3 Gyr and $[\text{Mg}/\text{Fe}] = +0.3$ signifying the duration of star formation less than 1 Gyr, the process had to be launched at $z = 0.4$. From this plot, we conclude that main star formation events both in the bulges and in the disks of the isolated S0 galaxies have no a single fixed epoch, but are homogeneously spread from very high redshifts to rather recent ones.

Two other plots of the Fig. 7 confront the chemical properties of the stellar populations to the dynamical parameter $(v^2 + \sigma^2)^{0.5}$, where v and σ are the rotation velocity and stellar velocity dispersion averaged over the disk-dominated or bulge-dominated area; this dynamical parameter characterizes, under the condition of virialization, the local gravitational potential. The correlation of the magnesium-to-iron ratio with the gravitational potential well, in particular, with the central stellar velocity dispersion, is well known for the elliptical galaxies (e.g. Trager, Faber, Worthey et al. (2000)). In our data, we see that the bulges (spheroids) and the disks behaves similarly as concerning the duration (the effectiveness?) of star formation in a particular gravitational potential well: the deeper the well the shorter star formation. However, the similarity of the bulges and disks disappears when

we inspect not the Mg/Fe ratio, but the global metallicity versus the dynamical parameter (Fig. 7, right plot): while the bulges follow the well-known mass–metallicity relation, the larger mass the higher metallicity, this correlation vanishes completely for the disks.

We can put our results on the stellar population properties in the bulges of isolated lenticular galaxies into a wider context by referring to the study of nearby lenticular galaxies with the integral-field spectrograph of the Russian 6-meter telescope, MPFS, by Sil’chenko (2006, 2008). In this work (Sil’chenko 2008) the data for the nuclei and bulges of more than 50 nearby S0s were presented; the sample included galaxies over a wide range of environments and was divided into two parts – ‘dense environments’ (Virgo cluster and central galaxies of rich groups) and ‘sparse environments’ (mostly peripheries of groups). In Fig. 8 we reproduce the Fig. 2 from Sil’chenko (2008) where we overplot our present results on the bulges of completely isolated S0s. Besides the data on the bulges of nearby S0s, this figure contains also mean relations for the integrated stellar populations properties of elliptical galaxies in clusters (Nelán, Smith, Hudson et al. 2005), in the field (Howell 2005), and in both types of environments (Thomas, Maraston, Bender et al. 2005). We must note here that among these comparison samples only ellipticals were considered by Howell (2005); Nelán, Smith, Hudson et al. (2005) and

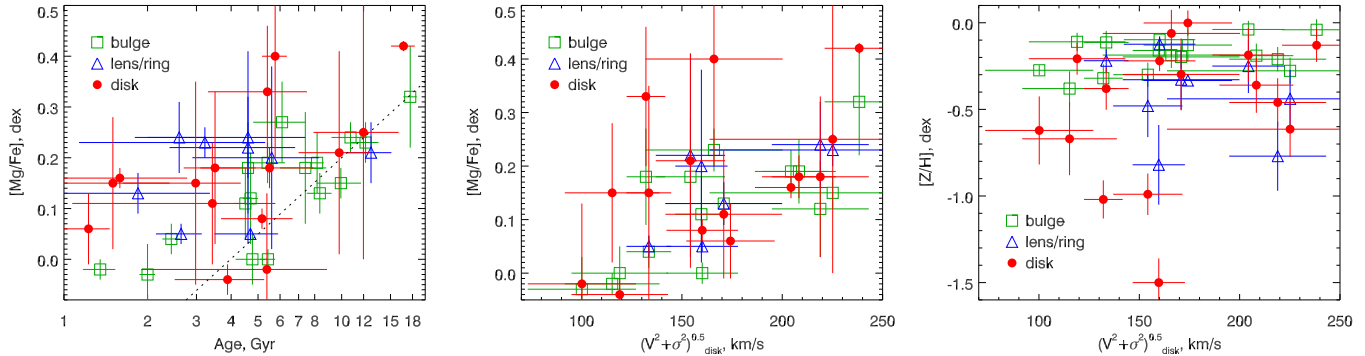


Figure 7. The relation age–Mg/Fe ratio (*left*), dynamical parameter $(v^2 + \sigma^2)^{0.5}$ versus alpha-element abundance (*center*), and some kind of the mass-metallicity relation (*right*).

Thomas, Maraston, Bender et al. (2005) have mixed ellipticals and lenticulars. In Fig. 8 we see that the relations connecting the ages and the [Mg/Fe] ratios with the stellar velocity dispersion found for spheroids in a wide range of environments are broadly consistent with our results on the bulges of isolated lenticular galaxies. However the stellar metallicities of the bulges are on average twice lower in the isolated S0s with respect to all other samples. We can speculate that this difference may be related to the possible difference in gas accretion sources in S0s galaxies in different environments, if the SSP-equivalent metallicity of the bulges is biased toward the metallicity of the last stellar generation born during some bulge rejuvenation event.

5.2. Rings and lenses

General structure of lenticular galaxies differs from that of other disk galaxies by often revealing such disk features as stellar rings (most frequent in S0/a, de Laparent, Baillard, & Bertin (2011)) and lenses (most frequent in S0s, Laurikainen, Salo, Buta et al. (2009)). It is a common view that the stellar lenses are very old and dynamically hot though this point of view is based on very rare observations of a few objects (Kormendy 1984; Laurikainen, Salo, Athanassoula et al. 2013). We have succeeded to measure kinematical and stellar population characteristics for 9 lenses and rings, and our results contradict to this common view. The stellar velocity dispersions are generally the same in the lenses/rings and in the surrounding disks (Fig. 9, right bottom plot) so dynamically they are indistinguishable; perhaps, there are some hints that the rings and lenses can be found mostly in dynamically hot disks. Fig. 9 gives also evidence for identical chemical properties of the lenses/rings and their surrounding disks. But there is however one important distinction between the disks and the lenses/rings: while the mean stellar ages of the disks fill out the complete range of possible values, between 1 and 12 Gyr, the ages of the rings and lenses are predominantly concentrated in the narrow range between 2 and 6 Gyr (Fig. 9, left upper plot). An exception is the galaxy from SCORPIO sample - NGC 6615 which has largest ring among entire sample with the age of ≈ 13 Gyr. We can so state that the last starforming episodes took place in these substructures at $z < 1$. Here we see an association with the fact that strong bars are predicted to appear in galactic disks only after $z = 1$ (Kraljic, Bournaud, & Martig 2012).

Since lenses in S0s are commonly related with dissolved or weakened bars (Buta, Laurikainen, Salo et al. 2010) and since star formation in rings is usual at the resonance radii of the bars (Buta & Combes 1996), we would like to connect the epoch of the last starforming episodes in the rings and lenses and the epoch of the rapid bar arising in the stellar disks after $z < 1$.

Another interesting finding can be seen in Fig. 10. While the bulges show the correlation between their ages and the stellar velocity dispersion, just as is known for elliptical galaxies, the disks and rings/lenses ages do not correlate with the observed stellar velocity dispersion. These findings are supported by the evaluation of Spearman correlation coefficient between the ages and velocity dispersion of the bulges, $r_s = 0.58$, with the probability of the correlation to be insignificant $p = 0.012$, while the correlation coefficients for the disks, $r_s = 0.07$, $p = 0.80$, and for the rings/lenses, $r_s = -0.17$, $p = 0.61$, prove that here the dependencies are absent. In addition, we found slight anticorrelation between the stellar metallicity and velocity dispersion in the ring/lens structures ($r_s = -0.46$, $p = 0.15$) while for the disks and bulges such correlation is insignificant ($r_s = -0.26$, $p = 0.34$ for the disks and $r_s = 0.12$, $p = 0.62$ for the bulges, correspondingly). It is obvious that such anticorrelation, if exists, has an evolutionary census; but extension of the galaxy sample with reliable measurements of the stellar population properties in the disk substructures is needed to strengthen the relation and to propose a particular scenario to explain it.

5.3. Ionized-gas characteristics

By analyzing the half of our sample observed at the Russian 6m telescope, we have noted that, firstly, the majority of isolated lenticular galaxies contain extended ionized-gas disks, and secondly, the rotation and orientation of the ionized-gas disks are often decoupled from the rotation and orientation of the stellar disks (Katkov, Sil'chenko, & Afanasiev 2014a). Now, with the complete sample in hands, we can refine the statistics of the ionized-gas content of the isolated lenticular galaxies. Among 18 galaxies studied, 13 galaxies demonstrate extended ionized-gas emission ($72\% \pm 11\%$); and among 13 galaxies with the extended gas emission, 7 galaxies ($54\% \pm 14\%$) demonstrate visible counterrotation of the ionized gas with respect to their stellar components. Our spectral observations are ‘one-dimensional’: the long slit

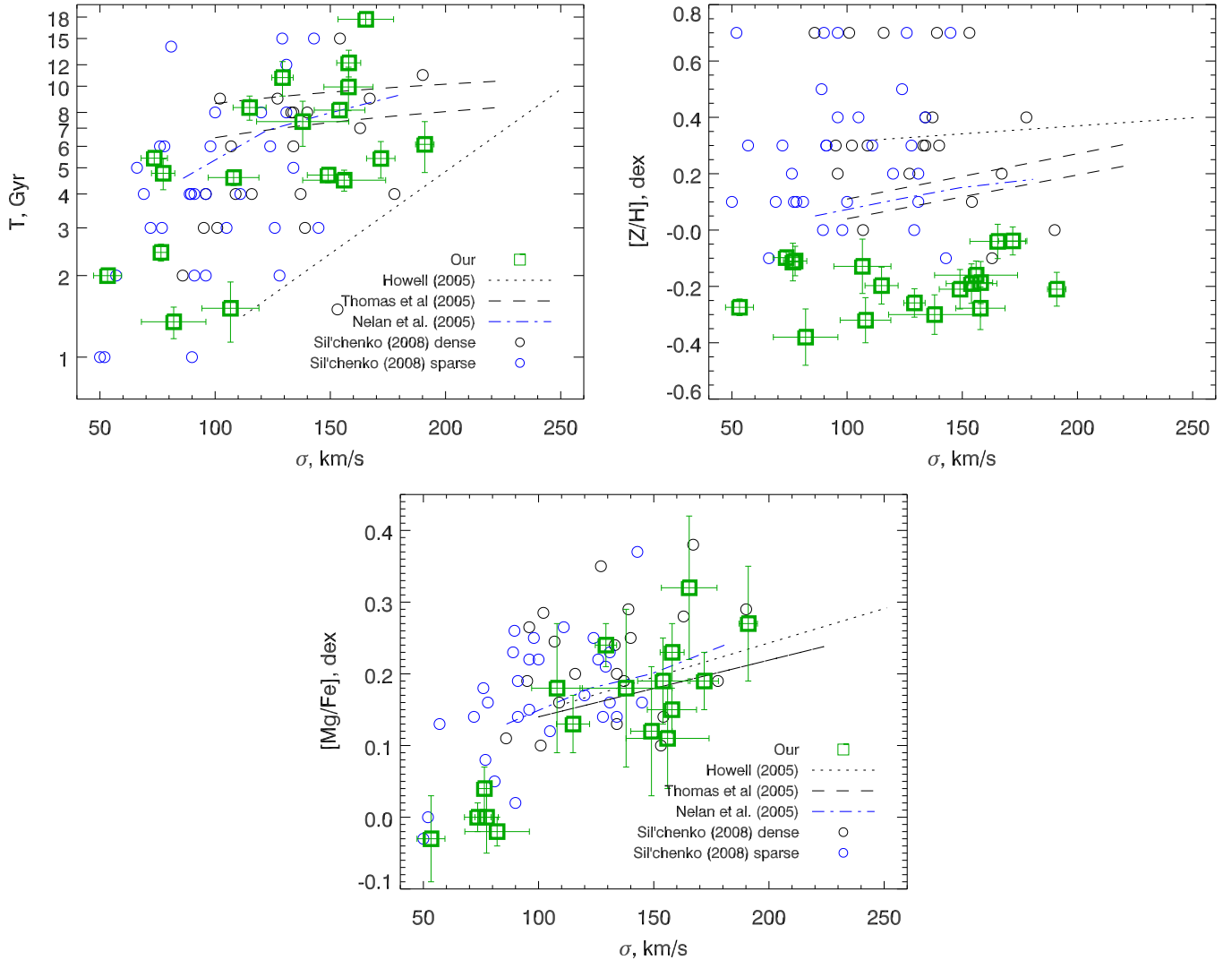


Figure 8. Comparison of the stellar population properties with the stellar velocity dispersion for the bulges of lenticular galaxies. Green squares shows our measurements in the isolated lenticulars; circles correspond to measurements from Sil’chenko (2008), colors code environmental properties of galaxies (*black* - dense, *blue* - sparse). Various samples of early-type galaxies from literature are also shown. Details see in Section 5.1.

aligned with the major axis of the continuum isophotes characterizing the line of nodes of the *stellar* disk cannot help to determine the orientation of the *gas* rotation plane. Following the logic proposed by Bertola, Buson, & Zeilinger (1992), if we suppose that the gas in S0s is accreted from external sources, and the orbital momentum of the accreted gas is oriented accidentally with respect to the angular momentum of the galaxy, we should see equal proportions of corotating and counterrotating gas by studying only the gas velocity projection onto the stellar disk lines of nodes. It is just what we have found from our observations of the isolated lenticular galaxies. So we may conclude that the statistics of the ionized-gas rotation in our sample of the isolated lenticular galaxies gives evidence for the *all* gas having been accreted from external sources isotropically distributed around the galaxies.

What can these sources be? Since our galaxies are *isolated* and do not have neighbouring large galaxies which may be donors of the gas, we can propose only two probable sources of the decoupled gas acquisition: minor merging of small gas-rich satellites (Reshetnikov & Sotnikova

1997; Bournaud & Combes 2003) or gas inflow from cosmological filaments of the Universe large-scale structure (Kereš, Katz, Weinberg et al. 2005; Dekel & Birnboim 2006; Bournaud & Elmegreen 2009). We suggest that metallicity of the gas can help to identify exactly the gas origin: cosmological filaments of the Universe large-scale structure must contain the pristine gas so it must be very metal-poor (Agertz, Teyssier, & Moore 2009). By pursuing this aim, we have picked out in our galaxies the radial ranges along the slit where the ionized gas is excited by young stars, according to the BPT-diagram diagnostics, and then we have added the spectra over these ranges for every galaxy. To these rather high-S/N spectra, we have applied so called ‘strong-line calibrations’ allowing to estimate oxygen abundance in the HII-regions with only a few emission lines, namely, with the Balmer lines $H\alpha$ and $H\beta$, low-excitation $[\text{NII}]\lambda 6583$, and high-excitation $[\text{OIII}]\lambda 5007$. We have succeeded to estimate metallicities of the ionized gas in 8 isolated lenticular galaxies. The results are presented in the Table 3. Despite the wide range of galaxy luminosities, the ionized-gas metallicities

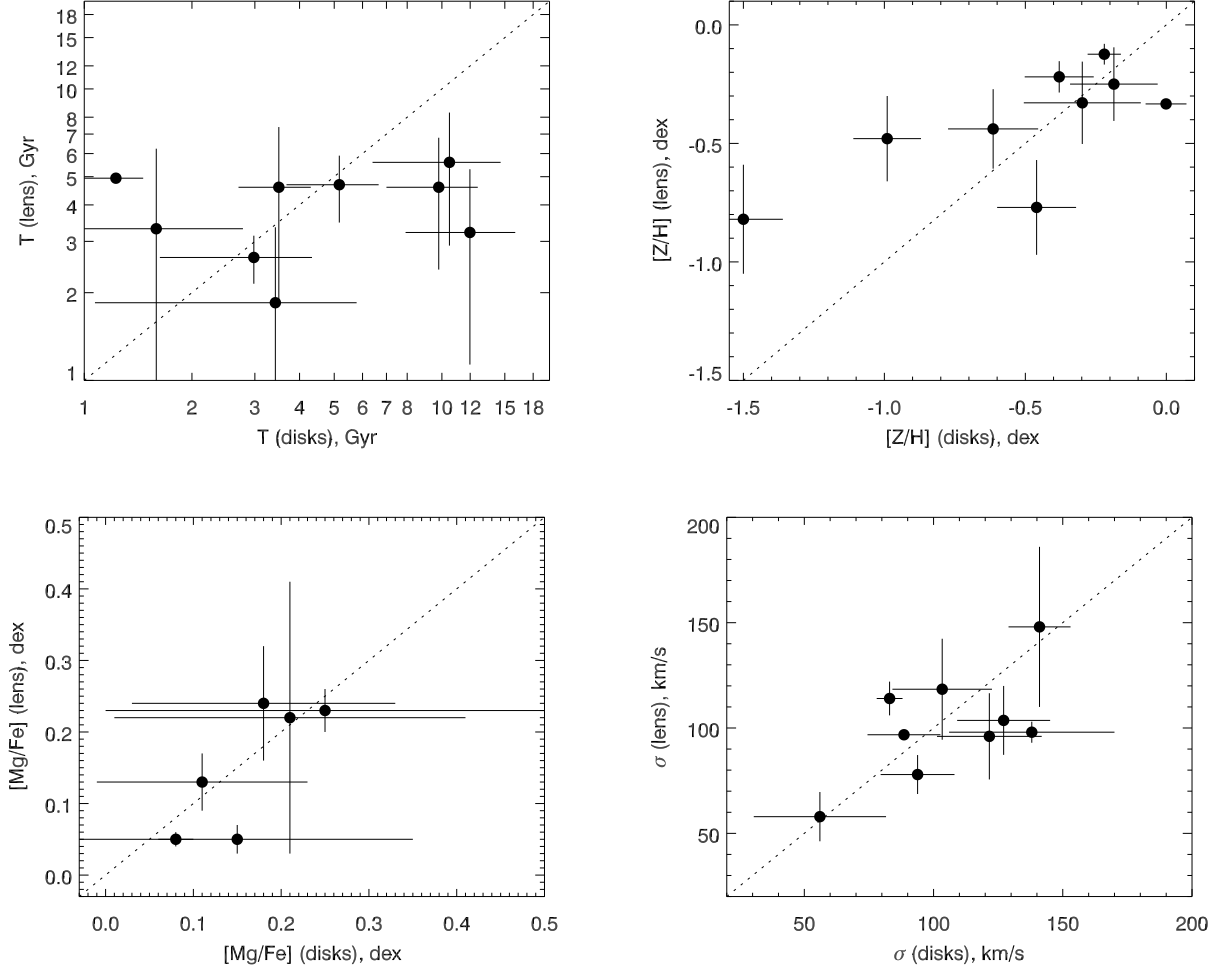


Figure 9. Comparison of the disks and their rings/lenses. Dotted line corresponds to equality line.

have appeared to be confined to a very narrow range of values near the solar metallicity or slightly higher. So we think that we can exclude cosmological filaments as the source of gas accretion in this particular case. Obviously, we see the consequences of gas-rich satellite merging.

Though formally we cannot determine the orientation of the ionized-gas rotation plane with the only long-slit spectroscopy, we can note some possible signatures of the gas confinement to the plane of the stellar disk: it may be consistency of the rotation velocity estimates for the stars and for the gas in the outer parts of the galaxies where the stellar velocity dispersion is low and does not affect strongly the line-of-sight velocity profiles through the asymmetric drift. Among our sample, such consistency is demonstrated by the galaxies with co-rotating ionized gas IC 1608, NGC 1211, NGC 2350, NGC 2917, UGC 9980, and by the galaxies with the *counterrotating* ionized gas NGC 4240 and NGC 6798; just these galaxies figure in the Table 3 with their outer ionized gas excited by young stars. Other galaxies where we can suspect the gas rotating off the main symmetry plane show mostly other types of excitation – by shock waves or by old post-AGB stars placing the emission-line flux ratios at the BPT-diagrams to the right from the dividing curve. We can here remind theoretical consideration

Table 3
Estimates of the ionized-gas oxygen abundance in the emission regions excited by young stars. $N2$ marks the estimations which has been done by using only $N2$ emission line index.

Galaxy	Radial range of binning, arcsec	$12+\log O/H$ ($[Z/H]_O$), dex
SALT-data		
IC 1608	(-51.4; -31.1)	8.78 (0.09) ± 0.47
	(29.7; 43.4)	8.80 (0.11) ± 0.26
NGC 1211 ^{<i>N2</i>}	(9.4; 15.8)	8.72 (0.03) ± 0.41
	(32.3; 37.3)	8.73 (0.04) ± 0.41
NGC 2917	(-15.7; -5.6)	8.90 (0.21) ± 0.27
	(9.6; 19.8)	8.82 (0.13) ± 0.26
NGC 4240 ^{<i>N2</i>}	(-11.6; -6.6)	8.80 (0.11) ± 0.41
	(4.1; 12.2)	8.78 (0.09) ± 0.41
UGC 9980 ^{<i>N2</i>}	(-13.1; -4.3)	8.82 (0.13) ± 0.42
	(8.4; 20.8)	8.71 (0.02) ± 0.42
SCORPIO-data		
NGC 2350	(-1.6; 2.0)	8.68 (-0.01) ± 0.25
NGC 6798 ^{<i>N2</i>}	(-34.1; -27.7)	8.71 (0.02) ± 0.41
	(29.1; 36.6)	8.73 (0.04) ± 0.41
NGC 7351	(-2.7; 3.8)	8.64 (-0.05) ± 0.25

by Wakamatsu (1993) who noted that inclined gaseous disks/rings must experience shocks developed because of

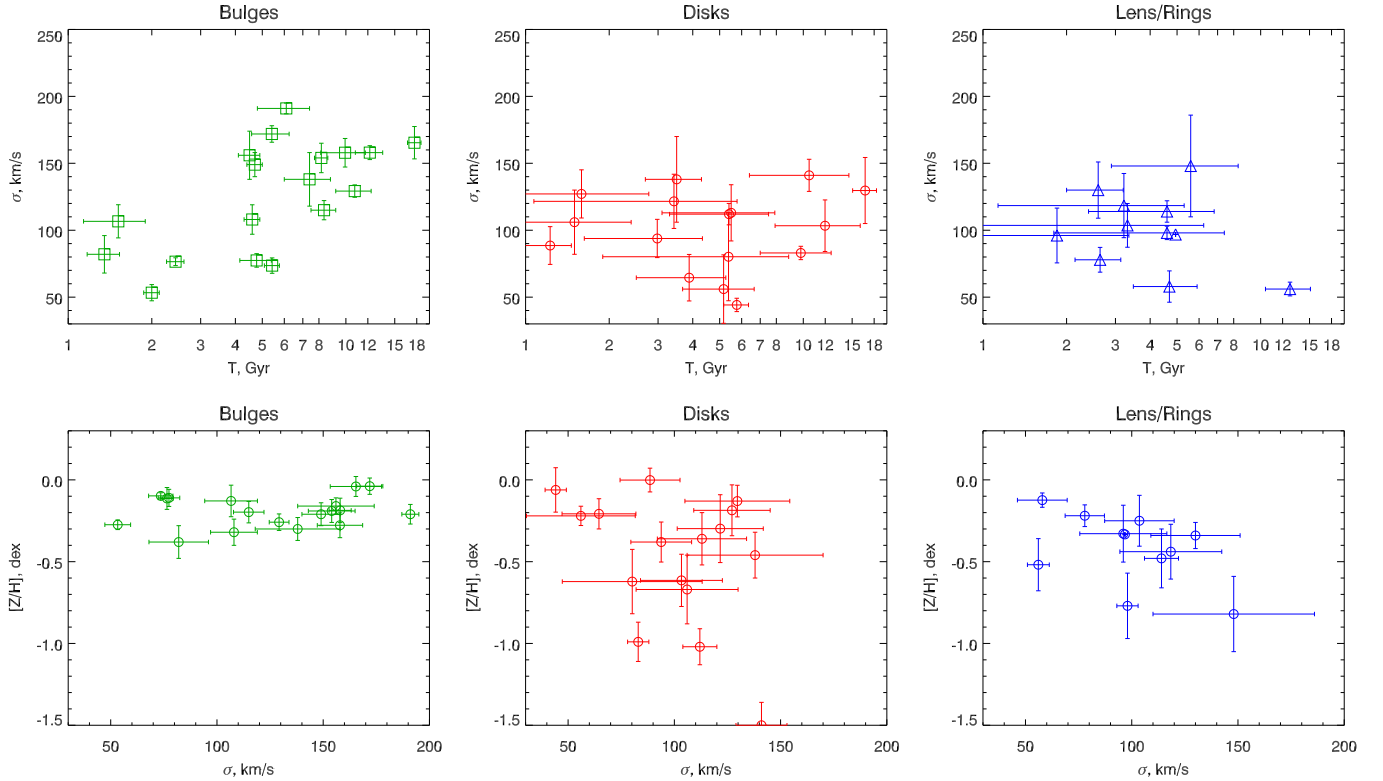


Figure 10. Parameters of the stellar populations for the joined sample SALT & SCORPIO targets.

the gas crossing gravitational potential well of a stellar disk. The shock waves must heat the gas and prevent its cooling necessary for a star formation burst. We suggest then that conditions for star formation starting in the accreted gas must include, besides the gas amount, also the favorable geometry of the gas accretion.

5.4. Origin of isolated S0s

Just from this point we would like to start discussion about the origin of isolated lenticular galaxies. Indeed, all the mechanisms proposed so far to quench star formation in the disks of spiral galaxies and to transform them into lenticulars act only in dense environments – in clusters and massive rich groups. It remained so quite unclear how lenticular galaxies in the field might form. The situation changes if we accept the new paradigm for evolution of disk galaxies proposed by Sil’chenko, Proshina, Shulga et al. (2012): all disk galaxies started their evolution as lenticulars at the redshifts of $z = 2 - 3$, and only after $z < 1$ most of them became spirals by undergoing persistent outer gas accretion onto their disks that resulted in dynamical cooling and subsequent spiral-arm development and star formation ignition. Then the key point for galaxy morphological shaping becomes outer-gas accretion regime. In clusters the outer cold gas accretion is almost impossible due to tide-induced starvation and hot intracluster medium ram pressure so in clusters the most disk galaxies remain lenticulars for all their lives. In the field the conditions for outer cold gas accretion can be quite various. If we regard gas-rich satellite merging as a main outer gas source, then we can expect the following variety of satellite system properties for the isolated disk galaxies: How many satellites has the host

galaxy? Are they distributed isotropically around it or are confined to some dedicated plane as it is observed in our Galaxy and in M 31? Is the satellite system dynamically cold or hot (related perhaps to the mass of the host dark matter halo)? Concerning the last point, there is a curious fact noticed by Karachentseva, Karachentsev, & Melnyk (2011). They considered faint companions of isolated galaxies from their catalog 2MIG. They found that the companions of isolated *early-type* galaxies have in average larger line-of-sight velocity difference with their hosts than the late-type ones. By inspecting their Fig. 4 we have ascertained that there is no practically companions of isolated early-type galaxies with the line-of-sight velocity difference less than 50 km s^{-1} while the isolated late-type hosts possess a lot of such companions. It is a natural suggestion that the accretion of companions with a large flyby velocity is more difficult than that of slow ones, so we come to a conclusion that perhaps just a ‘hot’ orbital population of companions defines an early morphological type of the host isolated galaxy. Perhaps, the orbital composition of a satellite system relates stochastically to initial conditions, or may be a present-day isolated lenticular have merged all its slow companions several Gyr ago and has no ones presently... In other cases, accretion of a gas-rich satellite from a highly inclined orbit may lead to gas heating and prevent star formation and spiral-arm development which requires cold, gravitationally unstable disk. By varying possible variants of satellite merging regime, we can easily get an isolated galaxy of any morphological type – in opposition to the tight accretion conditions in dense environments which provide a subsequent tight range of morphological types, mostly S0s.

6. SUMMARY

We have observed 9 galaxies from our sample of isolated lenticular galaxies at the 10m Southern African Large Telescope with the Robert Stobie Spectrograph in the long-slit mode. The radial variations of the kinematical characteristics, line-of-sight velocities and velocity dispersions, are studied both for the stellar component and for the ionized gas which is found in the most part of the sample. Also we have derived radial profiles of the mean stellar metallicity and ages, as well as the gas excitation characteristics and oxygen abundances far outward, into the disk-dominated regions of the galaxies. By joining two subsamples of isolated lenticular galaxies studied by us here and earlier, the northern and southern ones, with a totality of 18 isolated lenticular galaxies, we analyze the statistics of the stellar population properties and ionized-gas features for this morphological type of galaxies in extremely rarefied environments.

We have found that there is no particular time frame for shaping the isolated lenticular galaxies: the mean stellar ages of the bulges and disks are homogeneously distributed between 1 and > 13 Gyr, and the bulges and disks tend to form synchronously having mostly similar ages and magnesium-to-iron ratios. In some galaxies we have found stellar disk substructures – rings and lenses; their mean stellar ages are confined to a rather narrow range, from 2 to 5 Gyr. We relate the appearance of these structures to strong bars arising in disk galaxies after $z < 1$.

An ionized-gas extended emission is found in the majority of our galaxies, in 13 of 18 ($72\% \pm 11\%$). And the half of all extended gaseous disks demonstrate visible counterrotation with respect to their stellar counterparts. Just this proportion is expected if all the gas in isolated lenticular galaxies is accreted from isotropically distributed external sources. A very narrow range of the oxygen abundances, [O/H] from 0.0 to +0.2 dex estimated by us for the outer ionized-gas disks excited by young stars, gives evidences for the satellite merging as the most probable source of this accretion. At last we formulate a hypothesis that morphological type of a field disk galaxy is completely determined by the outer cold gas accretion regime.

ACKNOWLEDGMENTS

The observations reported in this paper were obtained with the Southern African Large Telescope (SALT). AYK acknowledges the support from the National Research Foundation (NRF) of South Africa. The study of isolated lenticular galaxies is supported by the grant No. 13-02-00059a of the Russian Foundation for Basic Research. IYK is grateful to Dmitry Zimin's non-profit Dynasty Foundation.

Funding for SDSS-III has been provided by the Alfred P. Sloan Foundation, the Participating Institutions, the National Science Foundation, and the U.S. Department of Energy Office of Science. The SDSS-III web site is <http://www.sdss3.org/>. SDSS-III is managed by the Astrophysical Research Consortium for the Participating Institutions of the SDSS-III Collaboration including the University of Arizona, the Brazilian Participation Group, Brookhaven National Laboratory, Carnegie Mellon University, University of Florida, the French Partici-

pation Group, the German Participation Group, Harvard University, the Instituto de Astrofísica de Canarias, the Michigan State/Notre Dame/JINA Participation Group, Johns Hopkins University, Lawrence Berkeley National Laboratory, Max Planck Institute for Astrophysics, Max Planck Institute for Extraterrestrial Physics, New Mexico State University, New York University, Ohio State University, Pennsylvania State University, University of Portsmouth, Princeton University, the Spanish Participation Group, University of Tokyo, University of Utah, Vanderbilt University, University of Virginia, University of Washington, and Yale University.

REFERENCES

- Agertz, O., Teyssier, R., & Moore, B. 2009, MNRAS, 397, L64. 0901.2536
- Baldwin, J. A., Phillips, M. M., & Terlevich, R. 1981, PASP, 93, 5
- Bertola, F., Buson, L. M., & Zeilinger, W. W. 1992, ApJL, 401, L79
- Binney, J. 1978a, Comments on Astrophysics, 8, 27
- Binney, J. 1978b, MNRAS, 183, 501
- Birboim, Y., Dekel, A., & Neistein, E. 2007, MNRAS, 380, 339. astro-ph/0703435
- Bournaud, F., & Combes, F. 2003, A&A, 401, 817. astro-ph/0301391
- Bournaud, F., & Elmegreen, B. G. 2009, ApJL, 694, L158. 0902.2806
- Buckley, D. A. H., Swart, G. P., & Meiring, J. G. 2006, in Society of Photo-Optical Instrumentation Engineers (SPIE) Conference Series, Society of Photo-Optical Instrumentation Engineers (SPIE) Conference Series, vol. 6267
- Burgh, E. B., Nordsieck, K. H., Kobulnicky, H. A., et al. 2003, in Instrument Design and Performance for Optical/Infrared Ground-based Telescopes, Society of Photo-Optical Instrumentation Engineers (SPIE) Conference Series, vol. 4841, eds. M. Iye, & A. F. M. Moorwood, 1463–1471
- Buta, R., & Combes, F. 1996, Fund. Cosmic Phys., 17, 95
- Buta, R., Laurikainen, E., Salo, H., et al. 2010, ApJ, 721, 259. 1008.0138
- Byrd, G., & Valtonen, M. 1990, ApJ, 350, 89
- Cappellari, M., & Emsellem, E. 2004, PASP, 116, 138. arXiv:astro-ph/0312201
- Cappellari, M., Emsellem, E., Krajnović, D., et al. 2011, MNRAS, 416, 1680. 1104.3545
- Chilingarian, I., Prugniel, P., Sil'Chenko, O., et al. 2007a, in IAU Symposium, IAU Symposium, vol. 241, eds. A. Vazdekis, & R. Peletier, 175–176. 0709.3047
- Chilingarian, I. V. 2009, MNRAS, 394, 1229. 0812.3272
- Chilingarian, I. V., Prugniel, P., Sil'Chenko, O. K., et al. 2007b, MNRAS, 376, 1033. arXiv:astro-ph/0701842
- Cid Fernandes, R., Mateus, A., Sodré, L., et al. 2005, MNRAS, 358, 363. astro-ph/0412481
- Crawford, S. M., Still, M., Schellart, P., et al. 2010, in Society of Photo-Optical Instrumentation Engineers (SPIE) Conference Series, Society of Photo-Optical Instrumentation Engineers (SPIE) Conference Series, vol. 7737
- Davis, T. A., Alatalo, K., Sarzi, M., et al. 2011, MNRAS, 417, 882. 1107.0002
- de Lapparent, V., Baillard, A., & Bertin, E. 2011, A&A, 532, A75. 1103.5735
- Dekel, A., & Birboim, Y. 2006, MNRAS, 368, 2. astro-ph/0412300
- Dressler, A. 1980, ApJ, 236, 351
- Faber, S. M., Friel, E. D., Burstein, D., et al. 1985, ApJS, 57, 711
- García-Appadoo, D. A., West, A. A., Dalcanton, J. J., et al. 2009, MNRAS, 394, 340. 0809.1434
- Gunn, J. E., & Gott, J. R., III 1972, ApJ, 176, 1
- Hau, G. K. T., & Forbes, D. A. 2006, MNRAS, 371, 633. astro-ph/0604452
- Howell, J. H. 2005, AJ, 130, 2065. astro-ph/0506424
- Hubble, E. P. 1936, Realm of the Nebulae
- Icke, V. 1985, A&A, 144, 115
- Illingworth, G. 1977, ApJL, 218, L43

- Johnston, E. J., Aragón-Salamanca, A., & Merrifield, M. R. 2014, *MNRAS*, 441, 333. 1403.5561
- Karachentsev, I. D., Karachentseva, V. E., Huchtmeier, W. K., et al. 2004, *AJ*, 127, 2031
- Karachentsev, I. D., & Makarov, D. I. 2008, *Astrophysical Bulletin*, 63, 299. 0812.0689
- Karachentsev, I. D., Makarov, D. I., & Kaisina, E. I. 2013, *AJ*, 145, 101. 1303.5328
- Karachentsev, I. D., Makarov, D. I., Karachentseva, V. E., et al. 2011, *Astrophysical Bulletin*, 66, 1. 1103.3990
- Karachentseva, V. E., Karachentsev, I. D., & Melnyk, O. V. 2011, *Astrophysical Bulletin*, 66, 389. 1112.2821
- Katkov, I. Y., Sil'chenko, O. K., & Afanasiev, V. L. 2014a, *MNRAS*, 438, 2798. 1312.6701
- Katkov, I. Y., Sil'chenko, O. K., & Afanasiev, V. L. 2014b, *Astrophysical Bulletin*, 69, 121
- Kauffmann, G., Heckman, T. M., Tremonti, C., et al. 2003, *MNRAS*, 346, 1055. astro-ph/0304239
- Kereš, D., Katz, N., Weinberg, D. H., et al. 2005, *MNRAS*, 363, 2. astro-ph/0407095
- Kewley, L. J., Groves, B., Kauffmann, G., et al. 2006, *MNRAS*, 372, 961. astro-ph/0605681
- Kniazev, A. Y., Zijlstra, A. A., Grebel, E. K., et al. 2008, *MNRAS*, 388, 1667. 0707.4288
- Kobulnicky, H. A., Nordsieck, K. H., Burgh, E. B., et al. 2003, in *Instrument Design and Performance for Optical/Infrared Ground-based Telescopes*, Society of Photo-Optical Instrumentation Engineers (SPIE) Conference Series, vol. 4841, eds. M. Iye, & A. F. M. Moorwood, 1634–1644
- Kormendy, J. 1982, in *Saas-Fee Advanced Course 12: Morphology and Dynamics of Galaxies*, eds. L. Martinet, & M. Mayor, 113–288
- Kormendy, J. 1984, *ApJ*, 286, 116
- Kormendy, J. 1993, in *Galactic Bulges*, IAU Symposium, vol. 153, eds. H. Dejonghe, & H. J. Habing, 209
- Kormendy, J., & Bender, R. 2012, *ApJS*, 198, 2. 1110.4384
- Kormendy, J., & Kennicutt, R. C., Jr. 2004, *ARA&A*, 42, 603. astro-ph/0407343
- Kraljic, K., Bournaud, F., & Martig, M. 2012, *ApJ*, 757, 60. 1207.0351
- Larson, R. B., Tinsley, B. M., & Caldwell, C. N. 1980, *ApJ*, 237, 692
- Laurikainen, E., Salo, H., Athanassoula, E., et al. 2013, *MNRAS*, 430, 3489. 1302.3019
- Laurikainen, E., Salo, H., Buta, R., et al. 2009, *ApJL*, 692, L34. 0901.0641
- Laurikainen, E., Salo, H., Buta, R., et al. 2010, *MNRAS*, 405, 1089. 1002.4370
- Le Borgne, D., Rocca-Volmerange, B., Prugniel, P., et al. 2004, *A&A*, 425, 881. astro-ph/0408419
- Makarov, D., & Karachentsev, I. 2011, *MNRAS*, 412, 2498. 1011.6277
- Makarov, D. I., & Karachentsev, I. D. 2009, *Astrophysical Bulletin*, 64, 24. 0908.1357
- Mitronova, S. N., Karachentsev, I. D., Karachentseva, V. E., et al. 2004, *Bulletin of the Special Astrophysics Observatory*, 57, 5. astro-ph/0408257
- Moore, B., Katz, N., Lake, G., et al. 1996, *Nature*, 379, 613. astro-ph/9510034
- Naim, A., Lahav, O., Buta, R. J., et al. 1995, *MNRAS*, 274, 1107. astro-ph/9502078
- Nelan, J. E., Smith, R. J., Hudson, M. J., et al. 2005, *ApJ*, 632, 137. astro-ph/0505301
- Ocvirk, P., Pichon, C., Lançon, A., et al. 2006, *MNRAS*, 365, 74. astro-ph/0507002
- O'Donoghue, D., Buckley, D. A. H., Balona, L. A., et al. 2006, *MNRAS*, 372, 151. astro-ph/0607266
- Pettini, M., & Pagel, B. E. J. 2004, *MNRAS*, 348, L59. astro-ph/0401128
- Prugniel, P., Soubiran, C., Koleva, M., et al. 2007, *ArXiv Astrophysics e-prints*. arXiv:astro-ph/0703658
- Quilis, V., Moore, B., & Bower, R. 2000, *Science*, 288, 1617. astro-ph/0006031
- Reda, F. M., Proctor, R. N., Forbes, D. A., et al. 2007, *MNRAS*, 377, 1772. astro-ph/0703545
- Reshetnikov, V., & Sotnikova, N. 1997, *A&A*, 325, 933. astro-ph/9704047
- Richter, O.-G., & Huchtmeier, W. K. 1987, *A&AS*, 68, 427
- Salpeter, E. E. 1955, *ApJ*, 121, 161
- Sancisi, R., Fraternali, F., Oosterloo, T., et al. 2008, *A&A Rev.*, 15, 189. 0803.0109
- Shaya, E. J., & Tully, R. B. 1984, *ApJ*, 281, 56
- Sil'chenko, O. K. 2006, *ApJ*, 641, 229. astro-ph/0512305
- Sil'chenko, O. K. 2008, in *IAU Symposium*, IAU Symposium, vol. 245, eds. M. Bureau, E. Athanassoula, & B. Barbuy, 277–280. 0709.2928
- Sil'chenko, O. K., Chilingarian, I. V., Sotnikova, N. Y., et al. 2011, *MNRAS*, 414, 3645. 1103.1692
- Sil'chenko, O. K., Kniazev, A. Y., & Chydakova, E. M. 2015. Submitted
- Sil'chenko, O. K., Proshina, I. S., Shulga, A. P., et al. 2012, *MNRAS*, 427, 790
- Spitzer, L., Jr., & Baade, W. 1951, *ApJ*, 113, 413
- Springob, C. M., Haynes, M. P., Giovanelli, R., et al. 2005, *ApJS*, 160, 149. astro-ph/0505025
- Sulentic, J. W., Verdes-Montenegro, L., Bergond, G., et al. 2006, *A&A*, 449, 937. astro-ph/0511652
- Thomas, D., Maraston, C., & Bender, R. 2003, *MNRAS*, 339, 897. astro-ph/0209250
- Thomas, D., Maraston, C., Bender, R., et al. 2005, *ApJ*, 621, 673. astro-ph/0410209
- Trager, S. C., Faber, S. M., Worthey, G., et al. 2000, *AJ*, 120, 165. astro-ph/0004095
- van den Bergh, S. 1976, *ApJ*, 206, 883
- van der Marel, R. P., & Franx, M. 1993, *ApJ*, 407, 525
- Wakamatsu, K.-I. 1993, *AJ*, 105, 1745
- Worthey, G., Faber, S. M., Gonzalez, J. J., et al. 1994, *ApJS*, 94, 687
- Worthey, G., & Ottaviani, D. L. 1997, *ApJS*, 111, 377

APPENDIX

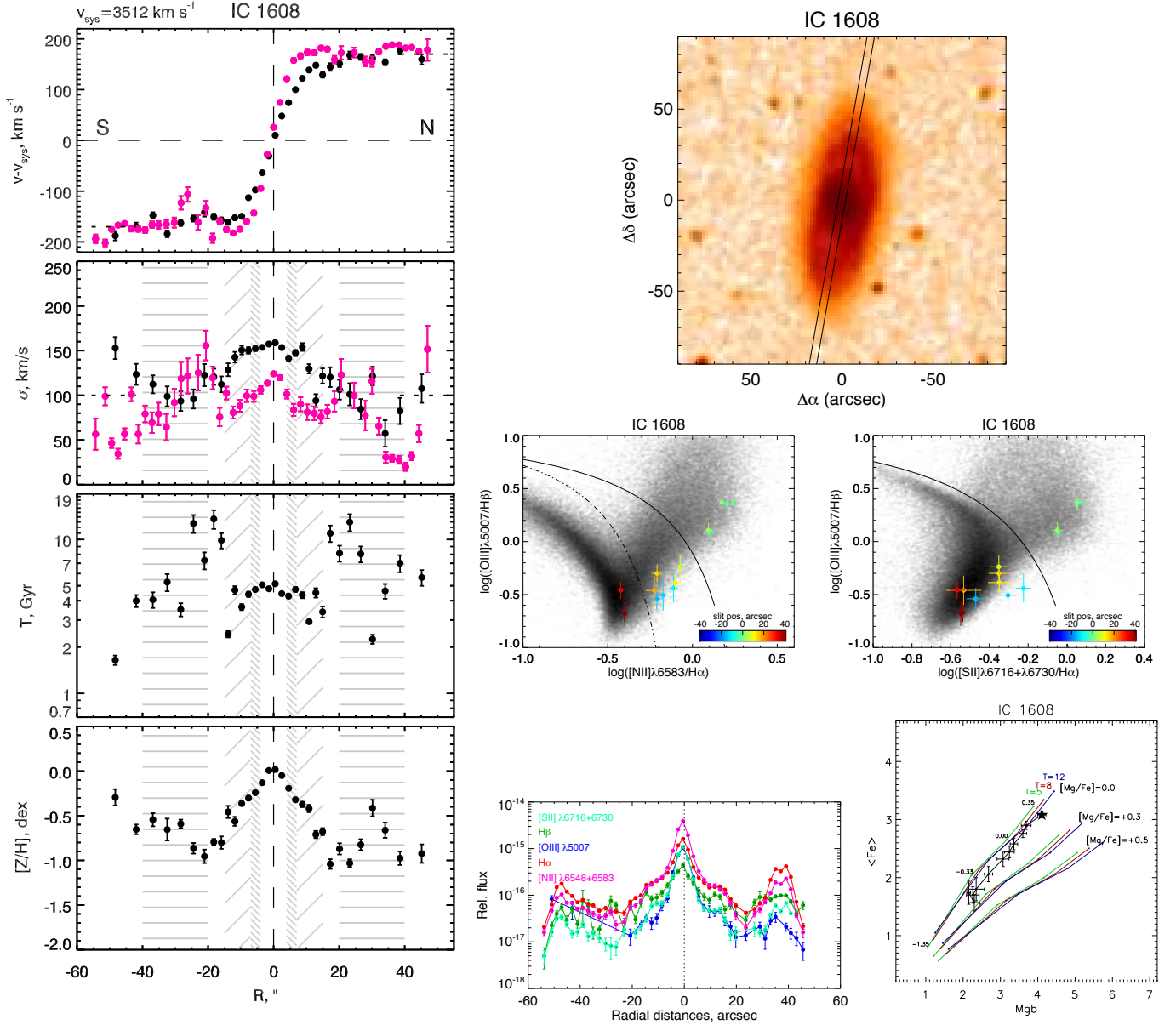


Figure 11. IC 1608. *Left block from top to bottom:* *i.* The radial profile of stellar (*black*) and gaseous (*pink*) line-of-sight velocity; *ii.* The stellar and gaseous velocity dispersion; *iii.* Properties of stellar populations – ages and metallicities. The shaded gray lines show radial segments where average stellar population parameters are calculated: ‘\’-like shading corresponds to bulge dominance regions, ‘/’ - to lens/ring regions, ‘/’ - to disk ones. *Right block from top to bottom:* *i.* Long-slit position superimposed on an (DSS) image of galaxy; *ii.* Excitation diagnostic diagrams comparing different emission-line ratios. The reference distribution of the measurements of the line ratios for galaxies from the SDSS survey with high signal-to-noise ratios ($S/N > 3$ in every line) are shown by gray color. The black curves, which separate the areas with the AGN/LINER excitations from areas with the star-formation-induced excitation, are taken from Kauffmann, Heckman, Tremonti et al. (2003) (*dash-dotted curve*) and from Kewley, Groves, Kauffmann et al. (2006) (*solid curve*). *iii.* Observed emission line fluxes. *iv.* Diagnostic diagram $\langle Fe \rangle$ versus Mgb. Points with error bars represent our measurements along the radius of the galaxy, starting from the nucleus marked by a large star. The SSP models by Thomas, Maraston, & Bender (2003) for three different magnesium-to-iron ratios (0.0, +0.3 and +0.5) and three different ages (5, 8 and 12 Gyr) are plotted as reference.

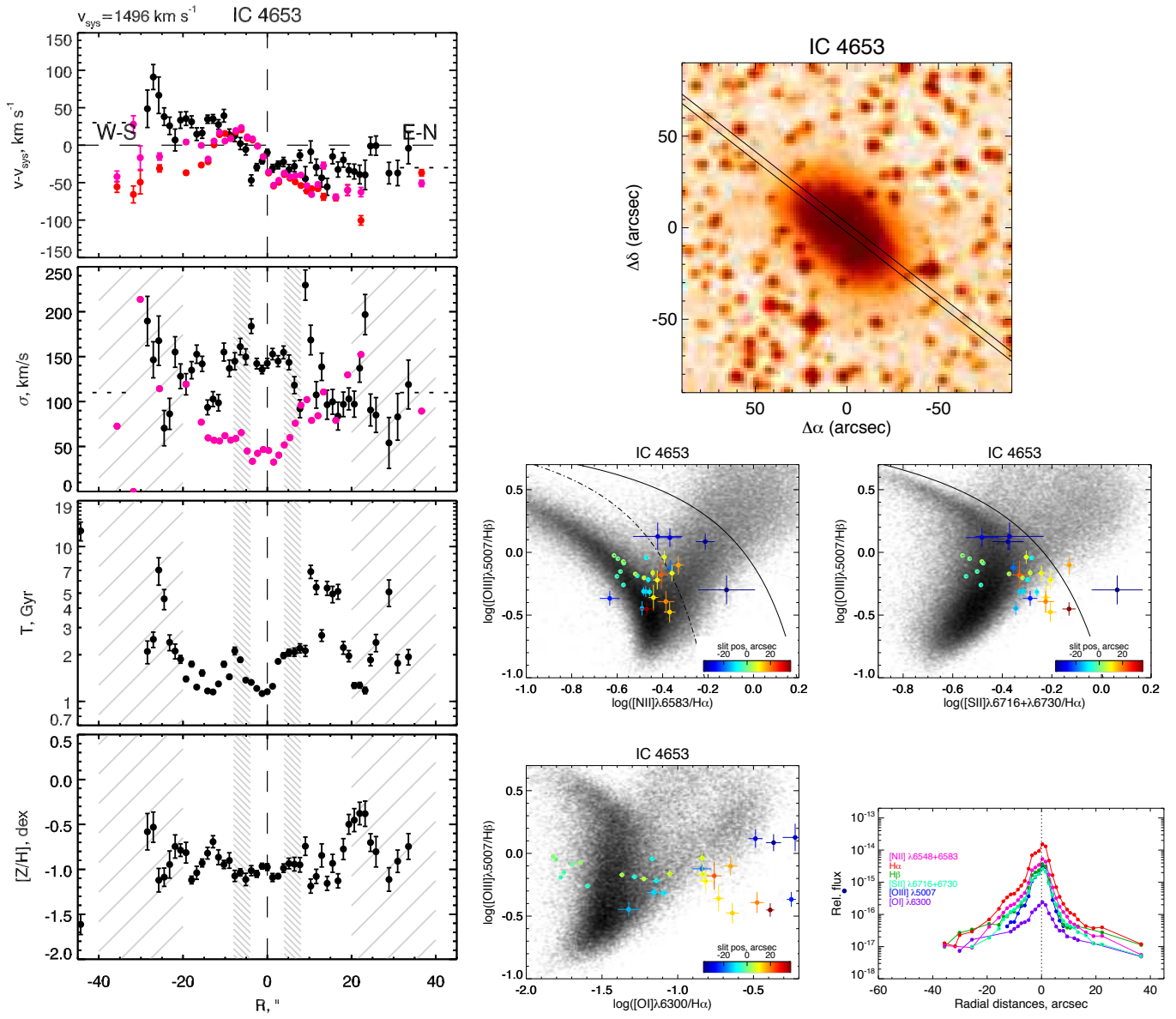


Figure 12. IC 4653. The same as previous figure.

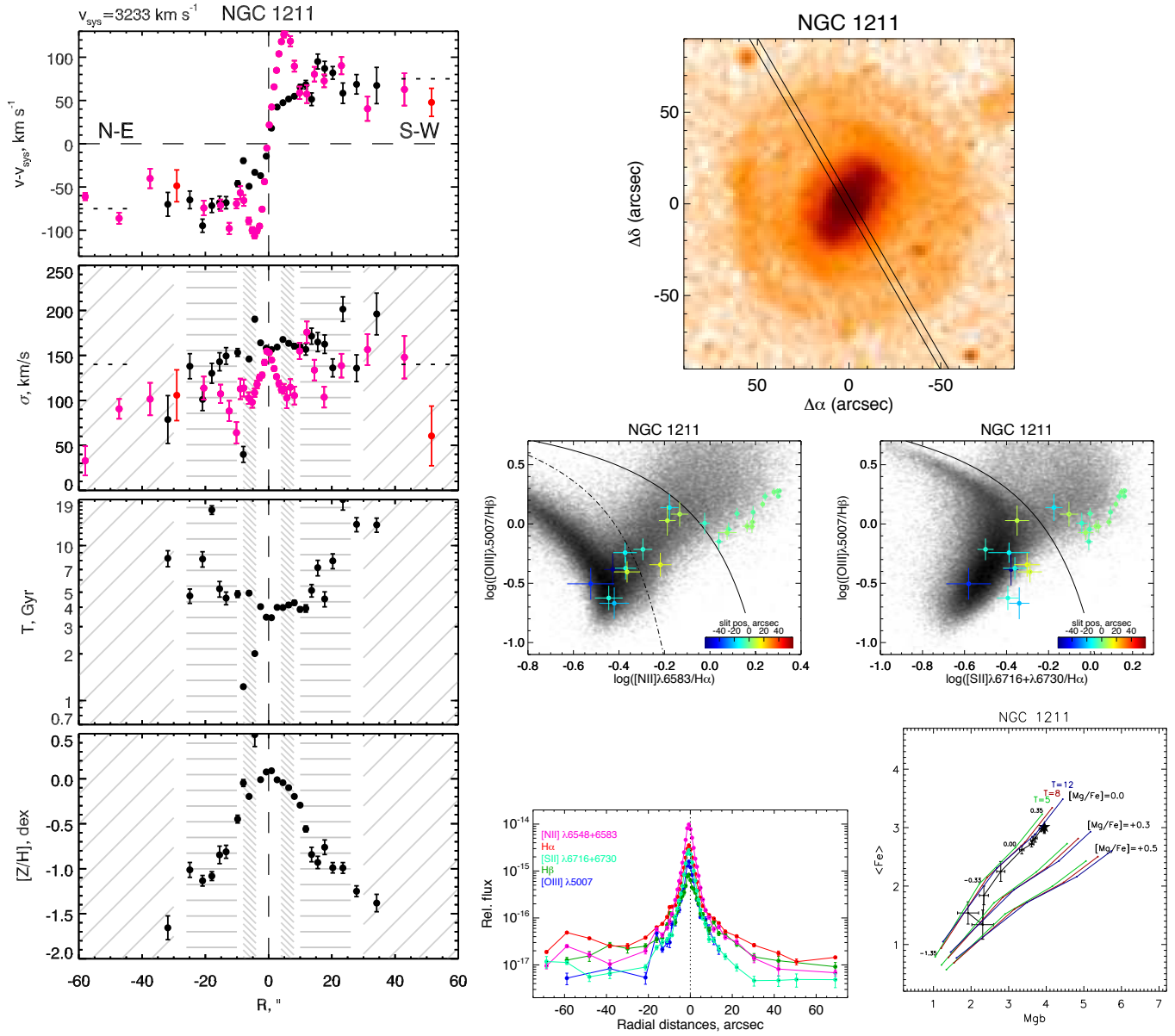


Figure 13. NGC 1211. The same as previous figure.

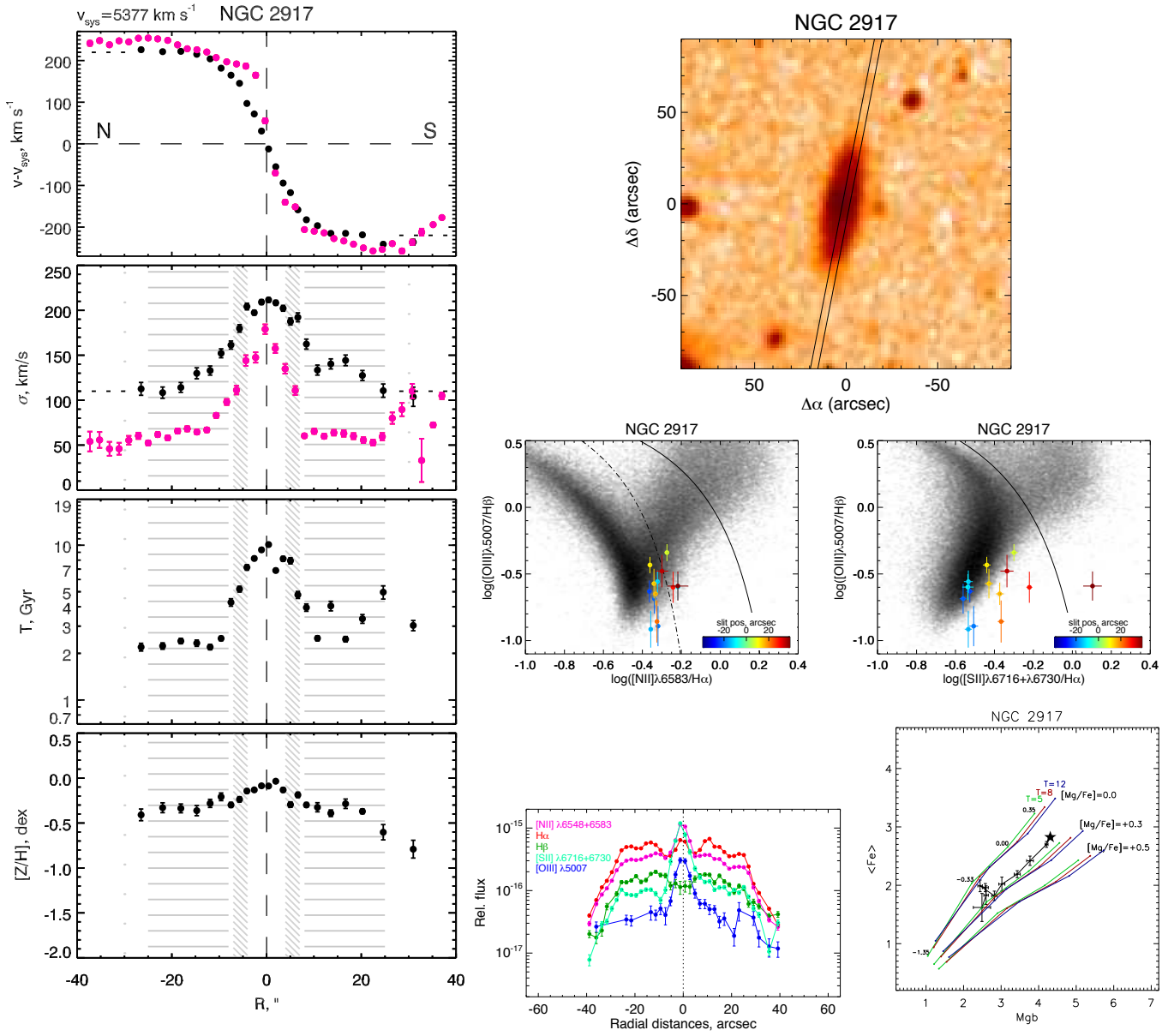


Figure 14. NGC 2917. The same as previous figure.

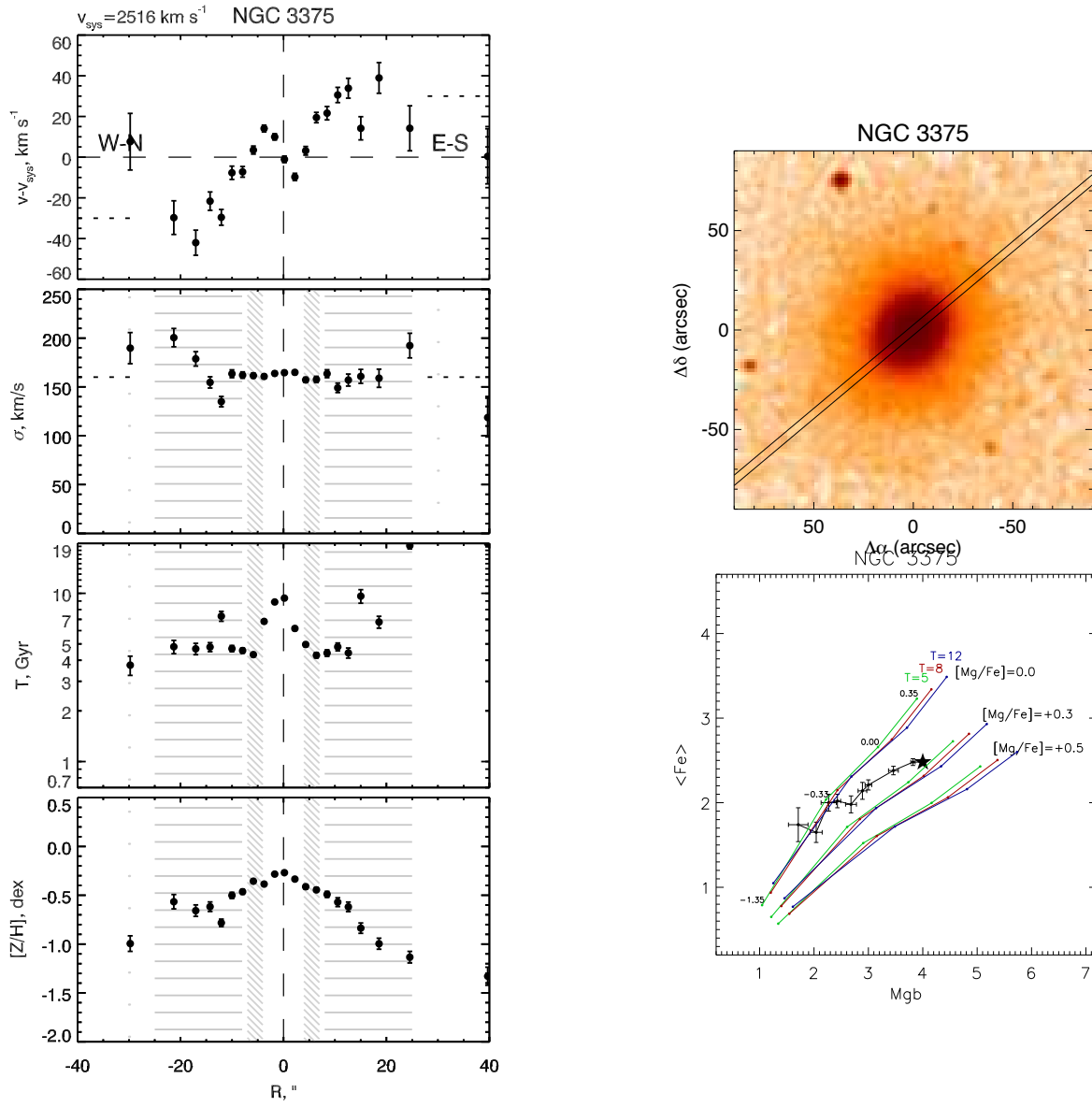


Figure 15. NGC 3375. The same as previous figure.

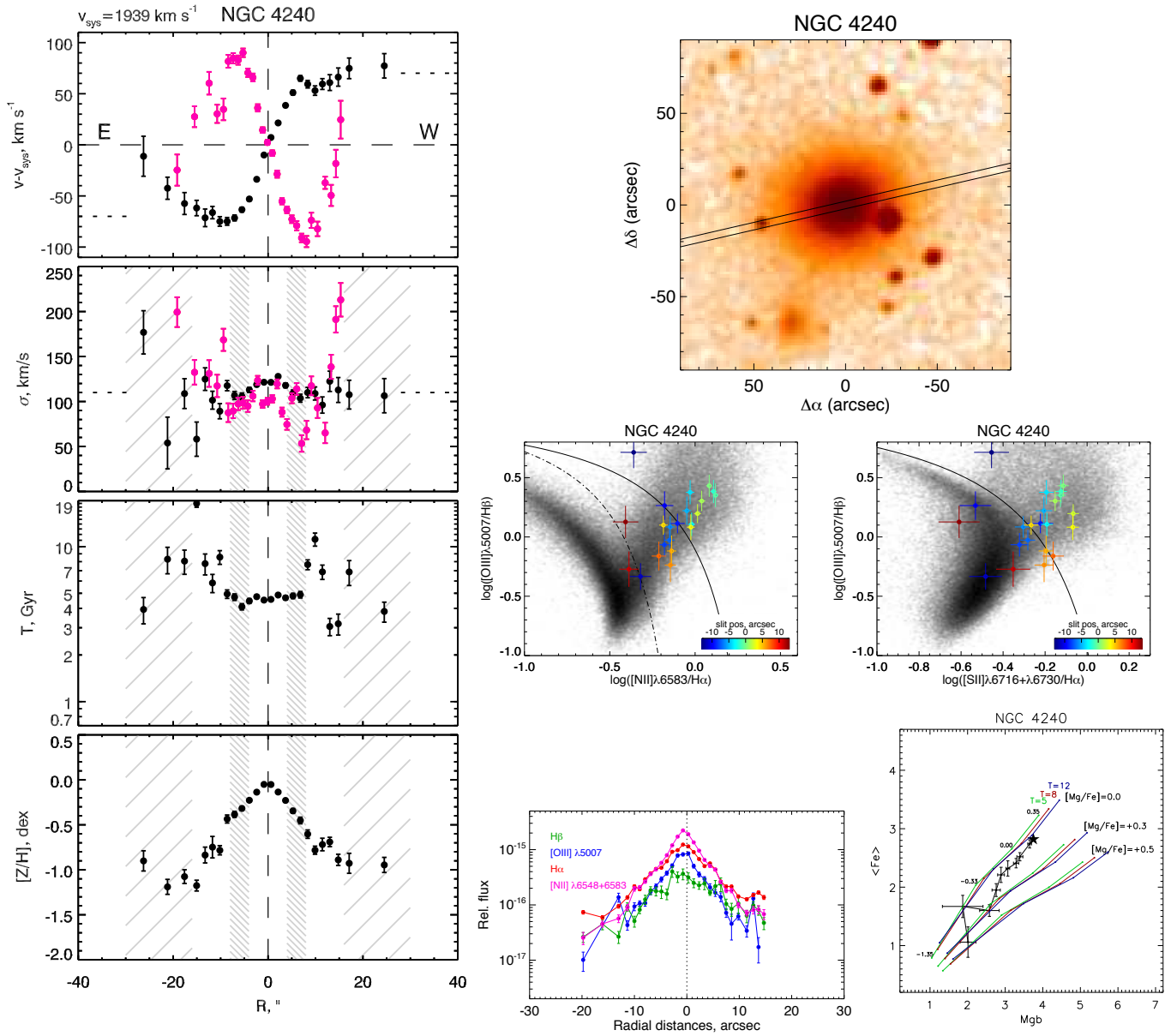


Figure 16. NGC 4240. The same as previous figure.

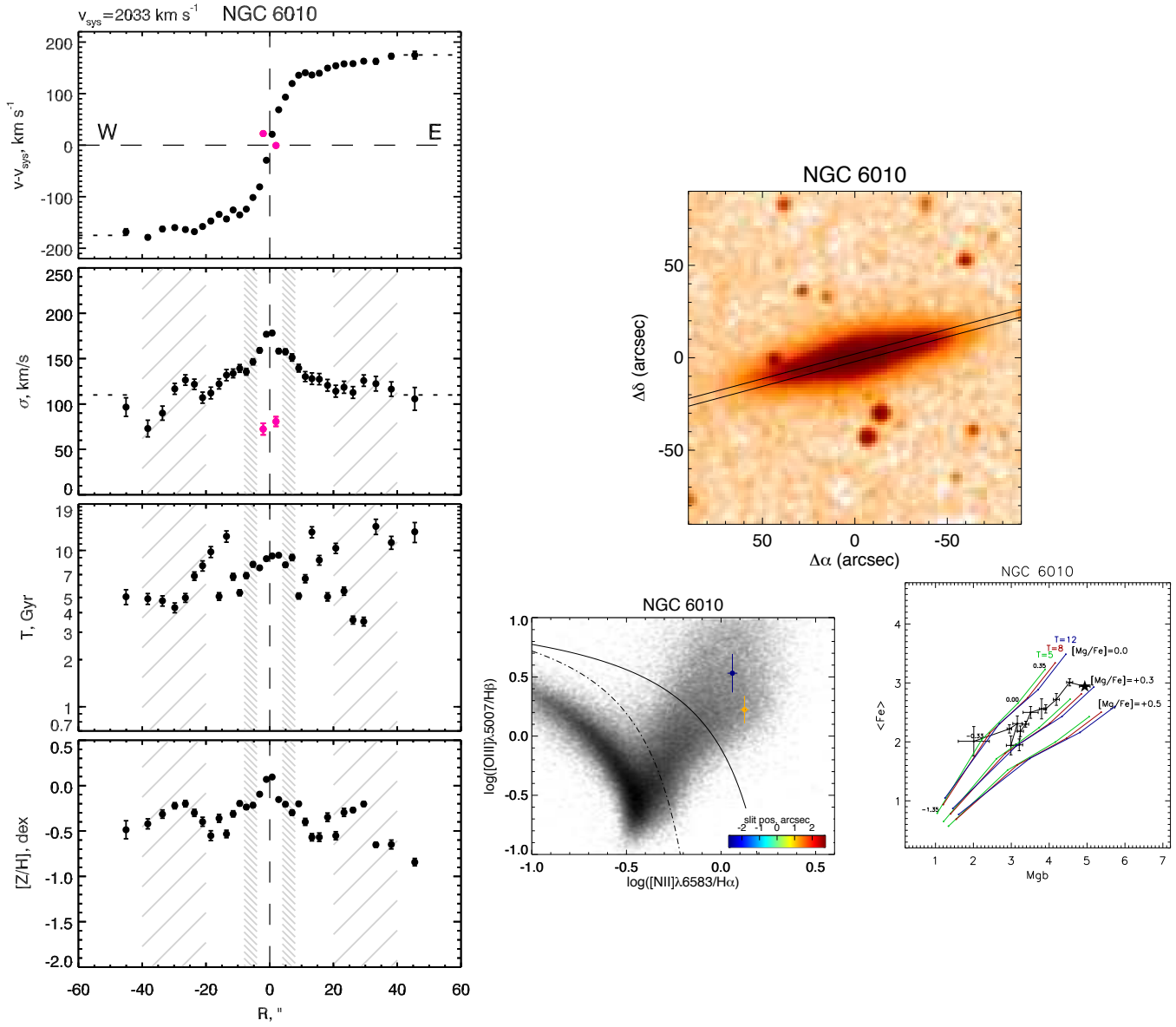


Figure 17. NGC 6010. The same as previous figure.

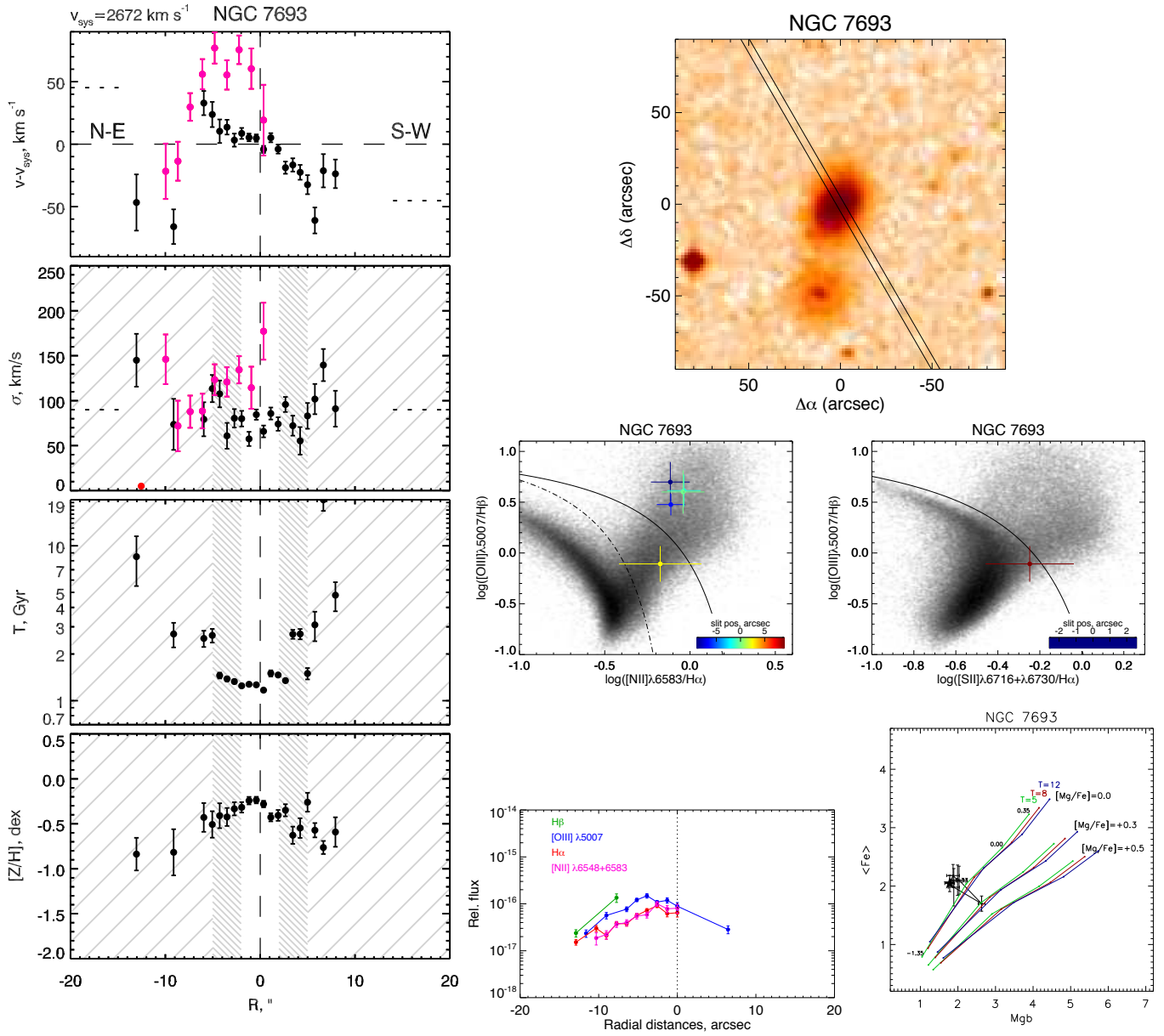


Figure 18. NGC 7693. The same as previous figure.

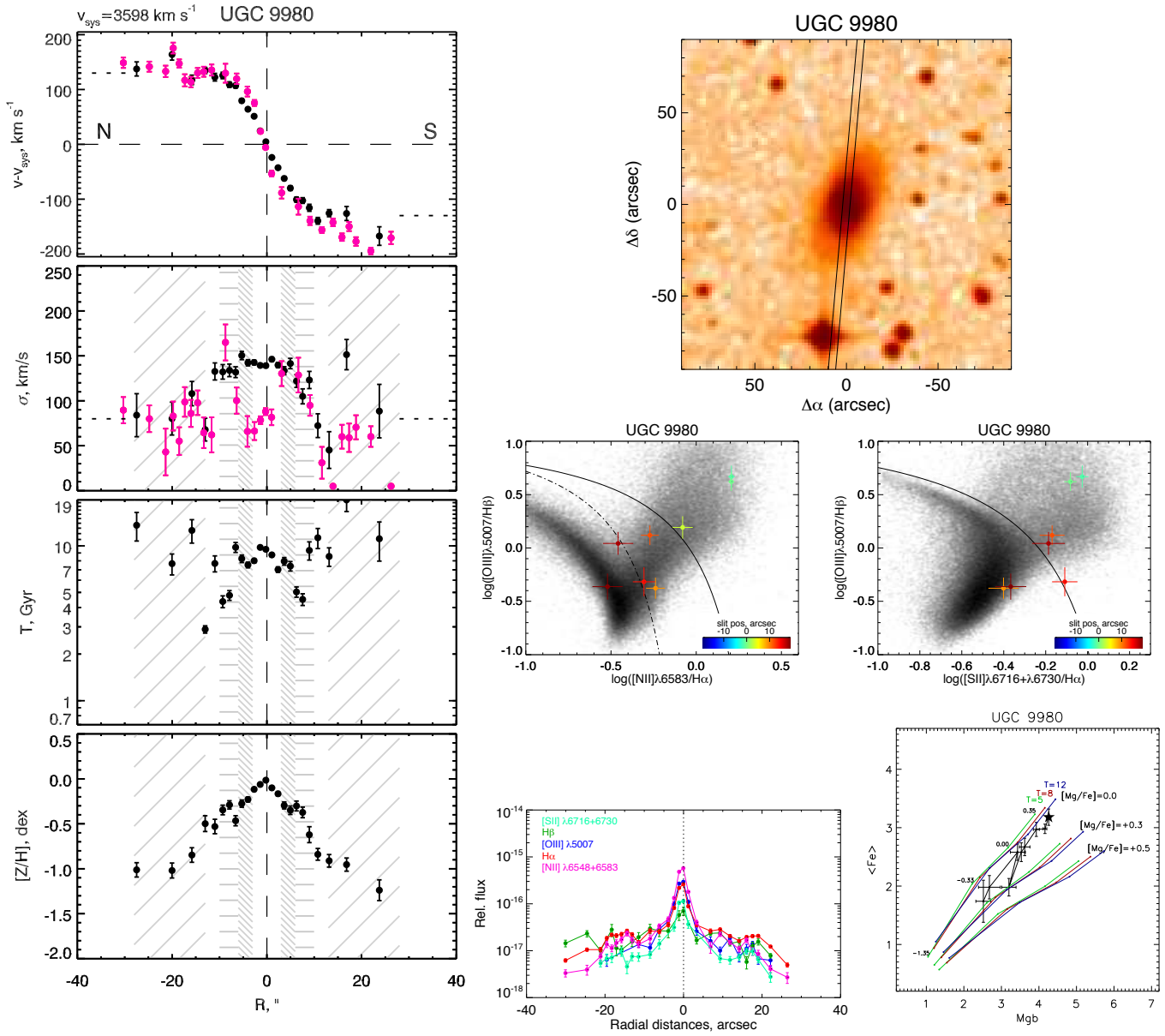


Figure 19. UGC 9980. The same as previous figure.